https://doi.org/10.1016/j.surfcoat.2016.02.019

Developments in laser-based surface engineering processes: with particular reference to protection against cavitation erosion

C.T. Kwok[a,b], H.C. Man[c], F.T. Cheng[c], K.H. Lo[a,b]

[a] Department of Electromechanical Engineering, University of Macau, China

[b] Institute of Applied Physics and Materials Engineering, University of Macau, China

[c] Department of Industrial and Systems Engineering, The Hong Kong Polytechnic University, Hong Kong, China

Abstract

With the increasing demands of economical, reliable and durable hydraulic and pneumatic systems, it is necessary to minimize the material damage from cavitation erosion (CE) when systems are handling cavitating and corrosive fluids. Cavitation erosion is a nausea for many engineering components, such as ship propellers & rudders, turbine, diesel engine, cylinder liner, pump impeller vanes, control valves, hydraulic turbines, bearings, pipes, ultrasonic cleaners, mechanical heart valves, etc, which are exposed to the high-speed flowing or vibratory fluids. This paper reviews the rationale behind the application of laser surface modification for achieving CE resistant surfaces of fluid handling components. The problem of CE may be tackled by enhancing the surface properties of the base materials (ferrous and non-ferrous alloys) with various laser surface modification techniques including laser transformation hardening (LTH), laser surface melting (LSM), laser surface alloying (LSA), laser cladding (LC), laser dispersion (LD) and laser plasma hybrid spraying (LPHS). The CE performance of a variety of laser-surface modified layers/coatings is discussed in this review. In particular, coatings of hard-facing alloys, shape memory alloys, surface metal or intermetallic matrix composites, cermets on ferrous and non-ferrous alloys are included. The mechanisms of the enhancement in cavitation erosion resistance (R_e) are discussed.

Keywords: Laser surface modification, Cavitation erosion, Corrosion, Synergism, Protection

1. Introduction

1.1 Cavitation erosion (CE)

Cavitation means the formation of bubbles or cavities in a liquid due to reduction in local pressure in the liquid. It is the consequence of Bernoulli's equation, which states that when the flowing speed of a liquid increases, its pressure decreases. When the local

pressure drops below a critical value, bubbles will form. When these bubbles encounter a high local pressure, they will implode, generating microjects or shock waves [1]. When the implosion of bubbles occurs near a solid surface, these microjects or shock waves impart intense pressure to the solid surface. Upon repetition of such events, the surface region under attack will undergo fatigue and rupture, with material loss from the surface. This is known as cavitation erosion (CE). CE is thus caused by the localized cyclic impact of fluid against a surface during the collapse of cavities. In metallic materials accumulated work-hardening and crack formation are commonly observed [2]. In some cases when the cavitation is intense, the density of cavitation pits is high enough to make a porous matrix and finally destroyed the component. Fig. 1 shows the cavitation damage in an impeller vane. Such damage will result in loss of pumping capacity and ultimately catastrophic failure of the pump impeller. On the other hand, hard brittle materials such as ceramics are unlikely to form a deep pit but cracking and spallation are the predominant failure modes.

There have been many attempts to correlate cavitation erosion resistance (R_e) to a single or a combination of mechanical properties of the metallic materials. These mechanical properties include ductility, hardness, ultimate tensile strength, yield strength, ultimate resilience, engineering strain energy, percentage of elongation [3] and product of fatigue strength coefficient and cyclic strain-hardening exponent [4]. However, the relations are empirical in nature and only provide prediction to a certain degree for a narrow group of materials. Owing to the repetitive, dynamic, stochastic and localised nature of the stress pulses produced by cavitation, the R_e of a material should be regarded as an independent material property on its own and not derivable from others [1]. Moreover, when the cavitating fluid is corrosive, the material loss is not purely mechanical in nature because corrosion also comes into play. When cavitation occurs in corrosive media, erosion-induced corrosion and/or corrosion-induced erosion will intensify the damage process and termed as 'cavitation erosion-corrosion' [5,6]. Erosion and corrosion often occur synergistically and material loss can be markedly higher than the sum of the effects of the processes acting separately [5]. An example of this can be found in the difference in CE rates between distilled water and 3.5 wt% NaCl solution [6]. In addition to the impact of corrosion on CE, it also can be speeded up by the synergistic effect due to erosive wear. Likewise, if the cavitating fluid contains erosive particles, then the collapsing cavities cause the particles to hit the surface at high speed. The erosion rate is higher than either cavitation corrosion or solid-particle erosion alone in hydraulic turbines operating in sandy water [7,8].

To mitigate CE, three approaches can be adopted including (i) improving design to minimize large hydrodynamic pressure differences; (ii) changing the environmental conditions, for instance, temperature and corrosivity of the fluids; (iii) selecting more

resistant material or applying a protective layer against CE. Unfortunately, it is not easy to change the design and control the environments while it is more feasible to use the third approach. Generally, the selection criteria of the CE resistant materials include hardness, work-hardenabililty, martensitic transformability (low stacking fault energy) for absorbing the cavitation energy, and corrosion resistance.

1.2 Laser surface modification

Since CE is a surface phenomenon, the R_e of a material is related to surface properties, but not bulk properties. Thus surface modification is a natural route employed in improving the R_e of engineering components. Surface modification has two unique features. Firstly, it uses only a small amount of costly coating material, with the bulk made of some cheaper material. Secondly, it allows a large number of combinations of surface and bulk properties, thus providing more flexibility for the design engineers. Surface modification of engineering alloys for combating CE has been attempted by various conventional techniques such as electroplating [9,10], electroless plating [11,12], electrospark deposition [13], microarc oxidation [14], cathodic-arc method [15], gas nitriding [16,17,18], plasma nitriding [19,20,21,22], friction surfacing [23], TIG surfacing [24], high velocity oxy-fuel spraying [25], plasma spraying [26], ion implantation [27,28,29,30]. However, there are limitations of these processes for fabricating protective layers or coatings on the substrate alloys, including weak adhesion bond to the substrate, high consumption of time and energy, environmental-unfriendliness, difficulty in automation, complicated heat-treating procedures, etc. Laser energy is a clean heat source which exhibits a unique set of properties such as monochromaticity, coherence, directionality and high intensity. It allows a wide range of surface treatments via heating of surface to melting of coating materials on the substrate through the absorption of the laser energy. The generic term ‘laser surface modification’ includes laser transformation hardening (LTH), laser surface melting/remelting (LSM), laser surface alloying (LSA), laser cladding (LC), laser dispersion (LD), laser glazing (LG) and laser shock peening (LSP). It is a technique for modifying the near-surface region of materials without changing the bulk properties. Compared with other surfacing methods, laser surface modification has derived its attractiveness and advantages for combating CE:

- It is a simple, economical and efficient process for materials surface leading to extended solid solution of alloy system, formation of metastable phases, homogenization and refinement of microstructure, and dissolution/redistribution of precipitates or inclusions while the bulk properties can be preserved.

- For LSA, LC and LD, strong metallurgical bonding between laser-fabricated layer and substrate is formed.
- The final surface obtained has a good chemical cleanliness and no chemicals or quenching medium is required.
- The heat-affected zone (HAZ) formed is small, leaving the bulk properties unchanged, with minimal distortion.
- Laser treatment process is clean and environmentally friendly.
- It is relatively easy to control the processing parameters and to be automated, and little or no machining is required.

On the other hand, the limitations of laser surface modification are:

- Finite beam size. This lowers the efficiency in treating a large surface. But large areas could be covered using diode lasers with rectangular spots as wide as one inch.
- Lower absorptivity of the laser in interacting with the metallic surface.
- It is a line-of-sight process. Thus it is not suitable for treatment of parts with very complicated geometry.

As stated above, one of the limitations of laser surface modification is the finite laser beam size. Currently, laser beams with spots as wide as one inch could be produced with diode lasers and/or adaptive optics. It is highly suitable for surface treating local regions and remanufacturing cracked, undersized, worn, corroded and cavitated engineering components.

2. Laser surface modification for combating CE

When the surface of a metallic material is irradiated by a laser beam, the energy is absorbed in a thin surface layer, thus resulting in rapid temperature rise in the surface layer only. The bulk of the substrate below the surface remains almost unaffected and hence acts as a heat sink, leading to rapid cooling or quenching of the surface layer as the laser beam passes. Depending on the substrate material and the presence or absence of added material, rapid heating and subsequent cooling of the surface layer may result in phase transformation, melting and resolidification, alloying or cladding. With appropriate choice of laser treatment process and processing parameters, the R_e of a metallic material can be significantly enhanced.

It is proposed that CE should be considered as a unique type of material damage in its own right. Although there is no general correlation between R_e of a material and its conventional mechanical properties [1], an appropriate combination of hardness and

toughness would likely result in a high R_e. [31]. A general observation of all these different treatments is that the new layer has a finer and more homogeneous microstructure, which is a favorable factor in resisting CE [55]. In the case in which additional materials are introduced into the surface layer, alloys with extended solubility and metastable phases may be formed, leading to further improvement in R_e. It is also observed that the R_e. of a material is closely related to, though not always totally determined by (the other factor is the microstructure), its microhardness (or more precisely, its indentation characteristics). This relationship is reasonable because the mechanical action of the imploding cavities on a solid surface is similar to the action of a microindenter or nanoindenter, though a single indentation parameter like microhardness is not completely adequate [73]. Based on this view, some degree of improvement of the R_e might be achieved by surface treatment to increase the microhardness. This paper is devoted to reviewing different laser surface modification processes of engineering alloys for the improving R_e.

Different laser surface modification methods employed in enhancing R_e are shown in Fig. 2. The first type is for microstructural modification of the surface without adding a new material including:

- laser transformation hardening (LTH)
- laser surface melting (LSM)

The others involve the addition of a new material to the near-surface region:

- laser surface alloying (LSA)
- laser cladding (LC)
- laser dispersion (LD) for forming surface composites
- laser plasma hybrid spraying (LPHS)

The working principles of laser surface modification are that the laser beam either in continuous or pulsed mode is focused into a suitable size and scans over the surface of the workpiece, and high energy density beam heats the surface rapidly for reducing the time for conduction into the bulk of the workpiece. The power density is defined as the power of the focused laser beam divided by the beam size. The interaction time is the length of time of the laser beam staying on any one point of the surface. Fig. 3 shows a range of laser surface modification that can occur at different power densities and interaction time [32]. It ranges from the low-power-density and long-interaction-time treatment (LTH) which relies on heating of a surface causing solid-state transformation without melting, to high-power-density and short-interaction-time treatment involving surface melting, which requires higher laser power for overcoming latent heat effects and larger conduction heat loss [32]. Simple surface melting can achieve more homogeneous modified layer (LSM) or very fast self-quenching (laser glazing) for the

formation fine grains, or even metallic glasses in some alloys. For the surface melting processes involving mixing with the added materials with different degree of dilution, they are classified as LSA, LC and LD. When very short pulses (short interaction time) of high power density was used to strike the surface, it is able to generate mechanical shock waves resulting in laser shock peening, which is similar to shot peening but with a shallower depth. However, attempts to enhance R_e via LSP are rarely reported, mainly because the modified depth is too small in industrial applications against cavitation attack in the long term. In addition, LSP in fact similar to cavitation attack, which is some kind of mechanical peening. Thus it is equivalent to the initial stage of CE, but in a controlled manner. In this sense it might not be considered as beneficial to R_e as it would shorten the incubation period.

2.1 Laser treatment without added material

In LTH and LSM, no additional material is introduced into the surface in the laser process. There is thus no change in the composition in the treated surface layer and the degree of change in properties that can be brought about is limited and substrate dependent. The studies of LTH and LSM for combating R_e and the results are summarized in Tables 1 and 2 respectively.

2.1.1 Laser transformation hardening (LTH)

LTH is an autogenous heat-treating method which involves solid-state transformation without melting. Laser energy absorbed by the material is controlled by the absorptivity of its surface. The ferrous alloys suitable for LTH include carbon steels, alloy steels, tool steels, martensitic stainless steels and pearlite cast irons with carbon contents ranging from 0.2 to 1.5 wt%. Generally, the alloys with high hardenability are processed with lower power density and a higher interaction time, in order to achieve a homogeneous case with significant depth. The ones with low hardenability are processed with higher power density and lower interaction times in order to ensure rapid cooling rates for martensite formation at the expense of a shallower case depth. The irradiated surface experience a quick heating and cooling cycles during which martensite will form. This martensitic phase introduces a higher hardness and hence higher CE resistance of the alloys. The hardness values obtained through LTH is about 20% higher than that of conventionally hardened ones. Depending on the alloys, hardness values up to about 1000 HV and case depths of 0.5 to 1.5 mm can be achieved. The local and controlled heat-input for LTH induces only very low distortion of the component, hence reworking of the component is not required. The rationale of LTH

lies in the possibility that a hardened surface would be more resistant to CE.

2.1.1.1 LTH of cast irons

The influence of LTH on the R_e of ductile iron, a material employed extensively for components in marine applications, including diesel-engine cylinder liners, valves and pumps. LTH of cast irons to improve R_e has been reported in a number of studies [33-36]. The degree of improvement varied, and was mainly determined by the compositions of the base material. In the studies on LTH of cast irons [33-35], the smaller increase in R_e seems to be attributable to a lower hardness. Li et al. [33] reported an improvement in R_e of about 1.9 times in the LTH of a high-phosphorous cast iron. It is generally concluded that the improvement in LTH is smaller compared with that in LSM because of a more refined and uniform microstructure, and a higher hardness, in the latter [33].

2.1.1.2 LTH of martensitic stainless steel

It has been reported that the hardness of AISI 440C treated by LTH could reach as high as 780 HV [36] in the hardened zone and the increase in R_e in 3.5 wt.% NaCl solution reached about 1.8 and 22.1 times as compared with conventionally heat-treated and as-received (annealed) 440C. The as-received 440C is composed of a ferritic matrix with coarse primary carbides (Fig. 4a(i)). The improvement in R_e for the laser-hardened 440C could be attributed to the presence of fine carbides and some retained austenite in the martensitic surface layer (Fig. 4b(i)) [36]. Compared with The as-received 440C, the degree of CE damage is less severe for the laser-hardened one as shown in Fig. 4a(ii) and 4b(ii).

Cast martenitic stainless steel 13Cr4Ni has found wide application in hydro turbines and LTH of 13Cr4Ni was reported by Mann [37]. The hardness of the laser-hardened 13Cr4Ni was 400 HV and the increase in R_e reached about 1.74 times as compared with the as-cast one. Both increased surface hardness and formation of fine-grained microstructure contributed to improvement in R_e of the laser-hardened 13Cr4Ni. R_e was found to be correlated with microstructure and mechanical properties such as ultimate tensile strength, modified ultimate resilience, and microhardness [37].

In a nutshell, the effectiveness of LTH for improving the R_e depends on the types of the ferrous alloys. The most significant improvement in R_e is observed in LTH of martensitic stainless steel AISI 440C due to the presence of fine carbides and some retained austenite in the martensitic surface layer with high hardness and toughness. Since no liquid phase is involved, the treated surface remains smooth.

2.1.2 Laser surface melting (LSM)

The application of LTH is somewhat limited as it can be applied only for alloys which are heat-treatable by laser. In addition, it is not accompanied by microstructural refinement as it does not involve solidification. LSM is performed by heating the surface of an alloy using a laser power density high enough to create a melt pool. From Fig. 3, as the power density decreases and interaction increases, the melting temperature of the alloy can be reached. Since a small portion of the top surface material is melted the cooling rate is very rapid, ranging from 10^3 to 10^6 °C/s depending on the thermo-physical properties of the alloy and the scanning speed of the laser. Among the various types of laser surface modification for enhancing R_e, LSM has been most widely reported because it is relatively simple and the increase in R_e could be quite significant. The R_e is increased due to the benefit of one or more of the following factors:

(1) grain refinement leading to an increase in hardness;
(2) removal of surface defects like inclusions and pre-existing pores or cracks;
(3) homogenization of microstructure, such as the conversion of coarse carbides into fine carbides; and
(4) formation of a hard and single-phase layer.

These factors will contribute to the formation of a hardened and more homogeneous surface. The increased hardness will improve R_e, while a more homogeneous microstructure contains fewer sites for the initiation of CE since in a multi-phase system, the R_e is determined by its weakest phase [38,39]. A number of studies on the effect of LSM of ferrous and non-ferrous alloys on R_e have been reported in the literature [33,34,40-51,53-57]. The improvement achieved in these studies is summarized in Table 2. On the other hand, laser glazing, which is a special type of LSM, involves surface melting followed by much more rapid self-quenching resulting in a very fine or amorphous microstructure. However, it is not reported in the literature probably because the treated layer is too thin and impractical for combating CE.

2.1.2.2 LSM of cast irons

LSM of cast irons for improvement in R_e was reported in a number of studies [33,34,40-43]. In the LSM of a high-phosphorous cast iron [33], the melted layer was ledeburitic and had a resistance 2.3 times that of the unmelted sample. On the other hand, LSM of a Cr-Mo-Cu alloyed cast iron [34] did not bring any significant increase in R_e. The CE behavior of cast irons modified by LSM in distilled water and in 3 wt.% salt solution was reported by Tomlinson's group [40-43]. The increase in R_e in distilled

water ranged from 2 to 20 times, depending on the type of cast iron treated, and was higher than in 3 wt.% NaCl solution. The improvement in R_e was attributed to the elimination of graphite flakes. The lower R_e in salt water originated from a significant contribution (about 70%) of corrosion-enhanced erosion to the overall erosion.

Gadag and Srinvasan [44] attempted LSM on ductile iron and reported an increase in R_e of at least 6 times in corrosive water media. The increase was mainly attributed to the formation of a ledeburite eutectic structure. Pearlitic ductile iron has only modest resistance to CE; the mean depth of penetration rate (MDPR) was 10-12 μm/h in distilled water. Ferritic ductile iron had consistently higher R_e than pearlitic iron, particularly in corrosive media. The CE rates in an aqueous slurry of 35 wt%, 220 grit SiC, synthetic sea water (3.4 wt%) and centi-normal dilute H_2SO_4 were 24, 40 and 86 μm/h respectively, whilst the corresponding rates were reduced to 3, 6 and 12 μm/h for laser-melted samples. The synergistic effect of corrosion and CE was more pronounced in the dilute acid than in the salt water. The CE rates decreased linearly with increase in the pH value of the cavitation bath. Laser treatment was very effective in bringing about a nearly seven-fold enhancement of R_e of ductile iron in mild corrosive media. This has enabled the delineation of the mechanism of CE of ductile iron before and after laser processing, particularly in corrosive baths.

2.1.2.3 LSM of steels

A number of groups reported their work on the LSM of steels for improving R_e [45-47]. The carbon steels (carbon content in the range of 0.20 to 0.45 wt.%) and the high-strength IRECA austenitic steel (Fe-17 wt%Cr-10 wt%Mn-9 wt%Co-3 wt%-0.1 wt% C-0.1 wt%N) [47] benefited from LSM treatment with an increase in R_e ranging from 2.8 to 5 times. The improvement in the case of carbon steels [45,46] originated from the formation of a hardened martensitic layer, while for the IRECA austenitic steel, from a refined microstructure.

2.1.2.4 LSM of stainless steels

Attempts of LSM on stainless steels have been undertaken by Preece and Draper [48] and Man's group [49-51]. In the study of LSM of austenitic stainless steel AISI 303 reported by Preece and Draper [48], the effects of surface roughening and residual stress dominated and the R_e of the laser-melted sample was lower than that of the untreated one. Among the three stainless steels modified by LSM reported by Kwok et al [49], only austenitic stainless steel S31603 (AISI 316L) had its R_e improved, and the amount was small (23 %). The presence of a tensile residual stress and a slight increase

in hardness were thought to be the causes for the improvement. On the other hand, LSM was detrimental to austenitic stainless steel S30400 (AISI 304) and super duplex stainless steel S32760 (Zeron 100) with respect to R_e. In the case of S30400, the R_e was slightly decreased, and was explained by the presence of a compressive residual stress, which is generally recognized as an unfavorable factor [52]. For S32760, the R_e was greatly reduced because of the presence of a high δ-ferrite content after remelting. While LSM of a martensitic stainless steel S42000 (AISI 420) led to an increase in R_e 1.8 times that achieved by conventional heat treatment [50]. The higher R_e was attributable to a high volume fraction of (89 %) of retained austenite combined with a moderate hardness (450 HV). In the LSM of AISI 440C [51], the microstructure of the laser-melted 440C consisted of martensite, retained austenite and carbides and its hardness was 430 HV. Compared with conventional hardening, the R_e achieved by LSM was improved in deionized water (by a factor of 1.95) but reduced in NaCl solution (by a factor of 0.48) although LSM could bring better improvement in corrosion resistance in NaCl solution [51].

2.1.2.5 LSM of copper-based alloys

Al bronzes are copper alloys extensively used as structural components in corrosive and erosive environments. These Al bronzes are multi-phase alloys containing a mechanically and chemically-weak phase. LSM of Al bronzes (C62400 and C62500) for enhancement of R_e was firstly attempted by Draper's group [53]. After LSM, the remelted layer consisted of a highly supersaturated single-phase structure. The incubation period was increased by an order of magnitude and the steady-state erosion rate was reduced by about 2.6 times.

LSM of manganese-nickel-aluminum bronze (MAB) (10.8 wt% Mn, 7.8 wt% Al, 2.2 wt% Ni, 3.6 wt% Fe), a common marine propeller alloy, was performed for improving the R_e by Tang et al [54,55]. In contrast to the complex and heterogeneous microstructure of as-received MAB (Fig. 5a(i)), the microstructure of the laser-melted MAB is highly refined and homogenized with a single β phase (bcc structure) (Fig. 5b(i)). The microhardness was increased to more than twice that of as-received MAB and the R_e in 3.5 wt.% NaCl solution was improved by 5.8 and 2.2 times compared with that of as-received MAB and nickel-aluminum bronze (NAB) (8.5 wt% Al, 5 wt% Ni, 4.5 wt% Fe), respectively. The improvement in R_e is attributable to increased hardness and also to a much more homogeneous microstructure. For untreated MAB, the cavitation attack started at the κ_I phase, followed by an attack at the α/β phase boundary during the initial stage and eventually developed into ductile tearing of the matrix (Fig. 5a(ii)). However, the laser-melted MAB only exhibited slight grain boundary attack at

the initial stage, being initiated from triple junctions (Fig. 5b(ii)). In addition, the damaged surface of the laser-treated samples showed fracture of a more brittle nature.

Cottam and his coworkers reported that the R_e of NAB after LSM (power = 1 kW, beam diameter = 3 mm, power density =14147 W/cm^2, scan speed = 25 mm/s) and 'laser processing' (power = 0.78 kW, beam diameter = 8 mm beam diameter, power density = 1551 W/cm^2, scan speed = 0.1 mm/s) was the same and higher than the as-cast NAB but the morphology of the eroded surfaces was different [56]. The nature of the CE for the as-cast NAB was preferential attack at the κ_{III} lamella. For the laser-melted NAB with the Widmanstatten structure, cavitation attack was preferential at the numerous grain boundaries and was more severe than that in the laser-processed one with larger equiaxed-grain structure. The tensile residual stress in the laser-melted NAB was found to be detrimental and negated its superior strength as compared with the laser-processed one. The deeper erosion and pitting in the laser-melted NAB could be attributed to the tensile residual stress, which accelerated the attack at grain boundaries.

2.1.2.6 LSM of titanium alloys

It has been reported that LSM of a titanium alloy Ti-6Al-4V in an inert gas (Argon) with martensitic structure was ineffective in improving the R_e [57].

From Table 2, it can be observed that for the cast irons, the increase in R_e was quite significant, ranging from 2 to about 20 times depending on the type of cast iron [33, 40-44]. For medium carbon steels, an increase of 2.8 times was reported [45,46]. For stainless steels, the results varied widely [48-51]. It can be observed from the summary that the improvement was most significant in cases where a hard surface layer was formed. This was the case when the alloy under treatment had a high carbon content to yield a martensitic layer, such as in the case of cast irons, carbon steels, and martensitic stainless steels. An exception was the IRECA steel reported in Ref. [47]. It was austenitic but it contained Co and behaved like Co-based alloy like the Stellites, which had high R_e. In other cases, such in multi-phase bronze, improvement after LSM resulted from microstructural refinement [53-56].

2.2 Laser treatment with added material

When additional material is introduced into the melt pool during laser surface modification, a new alloyed layer or a clad layer composed of the added material may be formed. The former process is known as laser surface alloying (LSA) and the latter is called laser cladding (LC). In fact there is a third possibility, that is laser dispersion

(LD) of hard reinforcement in the modified layer to form a surface metal-matrix composite (MMC) when the additional material introduced is a ceramic phase.

2.2.1 Laser surface alloying (LSA) and laser cladding (LC)

LSA is a tailor-made surface treatment applied on a base material for improving surface properties. In LSA, the added material melts and mixes with the molten substrate to form a new alloy. Typically, it involves melting of a thin layer of base metal with a high-power laser and simultaneously feeding an alloying element in form of powder or wire (co-deposition) into the laser generated melt pool [58]. On the other hand, various pre-deposition methods including physical/chemical vapor deposition, electroplating, thermal spraying, pasting, etc, can be used to preplace the material with desired thickness as a pre-deposited layer for LSA. The preplaced layer absorbs the laser energy leading to melting, intermixing with the substrate, rapidly solidified and finally bonded on the substrate. Since melting in LSA occurs in a very short time and only at the surface, the bulk of the substrate remains cool, thus serving as a heat sink. Large temperature gradients exist across the boundary between the melted surface region and the underlying solid substrate, resulting in rapid self-quenching and resolidification. This ensures formation of a strong metallurgical bond between the alloyed layer and the base material. An inert shielding gas is usually used to avoid oxidation during LSA process. When the coated material is immiscible with the base material, surface MMC will be formed instead of an alloyed layer. The phase with a lower melting temperature will melt and act as a matrix which embeds the unmelted phases for forming a surface MMC. Depending on the coating and substrate metallurgy, the surface layer can be tailored to the required composition and microstructure. The interaction time and laser parameters are important in determining the final microstructure.

When additional material is added to the melt pool for alloying or cladding, it mixes with the substrate material, that is, it is diluted by the substrate material. According to the specified parameters as shown in Fig. 6, the geometrical definition of ‘dilution’ of the laser formed layer is defined as [59]:

$$\text{dilution} = \frac{b}{h+b} \qquad (1)$$

where b is the thickness of substrate that was melted during the cladding process [mm], and h is the height of the clad bead [mm].

According to this definition, the smaller is the b or large is the h, the lower is the dilution. However, a thin layer of the substrate is always melted (to ensure metallurgical

bonding), 0% dilution is impossible. It is generally agreed that a dilution value equal to or less than 10% is needed for cladding in the real sense. For higher a dilution value, it is classified as LSA as there is non-negligible amount of substrate material in the surface layer. Note that dilution is a quantity that is meaningful only for LC since the goal in cladding is to cover the substrate with another material. In LC with cladding material introduced by powder injection, it is difficult to determine the dilution.

When the dilution is higher than 20% (high degree of dilution), it is considered as LSA. When the dilution of the solidified surface is smaller than 10% (low degree of dilution), the laser process is termed LC, and the properties of the cladding material are considered to be retained. LC enables cladding materials to be bonded to the substrate with minimum mixing between the cladding and the substrate. LC produces a relatively thick and homogeneous overlay of coating material on a substrate with a fusion bond.

Obviously, LSA and LC are much more complicated than LTH and LSM, both in terms of the processing parameters and the microstructures formed. On the contrary, these processes are more versatile and effective than LTH and LSM. There are numerous studies reporting on the modification of ferrous and non-ferrous alloys for enhancing R_e using added materials [60-87]. In general, the degree of improvement achieved is higher than that in LTH and LSM.

2.2.1.1 LSA of cast iron

LSA of flake graphite grey cast iron using Cr, Ni and Co for enhancing R_e was reported by Tomlinson and Bransden [60,61]. R_e was considerably increased in all cases in both distilled water and 3 wt.% NaCl solution, with Cr producing the highest resistance (25 and 9 times that of cast iron, respectively). The high R_e in the case of Cr alloying was attributed to the formation of a fine microstructure composed of austenite and ferrite.

2.2.1.2 LSA of carbon steels

LSA of carbon steels using Ni-based and Co-based hardfacing alloys was attempted by some research groups [62,63,64], with various degrees of improvement in R_e. The improvement resulted from a fine microstructure and increase in hardness. Szkodo's group reported the CE of laser-alloyed AISI 1045 carbon steel and 13% chromium steel (2Cr13) in water at 25 ^{o}C [65,66]. High R_e of the laser-alloyed layers is linked to their microstructural features and does not reflect values of their mechanical

parameters. Microstructure composed of austenite skeleton filled with martensite is the most susceptible to strain hardening under cavitation loading. Such a microstructure was found to be the most cavitation resistant at low intensity of loading. Increase in hardness in martensite is accompanied by inevitable increase in brittleness and decrease in capability in absorbing impact energy [64]. Microstructure composed of chromium carbide and molybdenum carbide skeleton surrounding the martensite cells is the most resistant to plastic deformation at high intensity of loading [66]. This kind of microstructure warrants the longest incubation period but the highest volume loss rate of erosion, in the next stage of CE, due to low impact toughness. R_e of austenite with large amount of chromium carbides is the worst due to high brittleness of such a microstructure and low resistance to plastic deformation under cavitation loading [66].

LSA of mild steel AISI 1050 using AlFeSi powder was attempted by Kwok el al [67]. The maximum hardness achieved for laser-aluminized layer was 595 HV. The R_e of the laser-aluminized specimens was much higher than that of the substrate (about 17 times) due to the presence of Fe_3Al, FeAl, and solid solution hardened α-ferrite. Although alloying of aluminum to the steel led to an active shift in the free corrosion potential, the laser-aluminized specimens showed passivity while the steel substrate did not.

2.2.1.3 LSA/LC of stainless steels

Laser surface modification of austenitic stainless steel AISI 316L using various elements (Co, Ni, Mn, C, Cr, Mo and Si) and alloys or compounds (AlSiFe, NiCrSiB, NiCoCrB and Si_3N_4) was reported in a number of studies by Kwok et al [68,69,64]. The highest increase in R_e is 12 folds. The improvement could be explained in terms of (i) increase in hardness due to solid solution hardening and formation of hard phases such as carbides, borides and intermetallics, (ii) decrease in stacking-fault energy (SFE), and/or enhanced strain-induced martensitic transformability, thanks to the presence of certain elements such as Co. In comparison, LSM of 316L stainless steel could only bring about minimal increase in R_e (20 %). The increase was much higher by LSA [55, 57, 58, 63].

Szkodo reported the cavitation performance of X5CrNi18-10 stainless steel (max 0.08 wt.% C, max 2 wt.% Mn, 18 wt.% Cr, 9 wt.% Ni) with Fe-Cr-Mn and Fe-Cr-Co alloys which are frequently used in power plants for routine repairs of damaged blades working under cavitation loading [70]. Results revealed that microstructural refinement due to laser processing contributes to delay of austenite-to-martensite phase transformation. Kinetic of austenite-to-martensite transformation is different for investigated alloys and depends on the chemical composition and laser processing

conditions.

LC of Stellite 6 (Cr 28.2 wt%,W 4.3 wt%, Ni 1.1 wt%, Fe 1.4 wt%, C 0.92 wt%, Co-bal.) on stainless steel 13Cr–4Ni (C 0.06 wt%, Si 0.3 wt%, Mn 0.65 wt%, P 0.03 wt%, Cr 12.8 wt%, Ni 4.1 wt%) has been performed at varied laser energy densities to study the CE in 3.5 % NaCl solution [71]. Variation of laser energy density from 32 to 52 J/mm^2 changed the compositions in the clad such that the Fe and Ni contents increased whereas Co, Cr, and W contents were reduced. Cladding at 32 J/mm^2 showed higher hardness (705 HV) and higher R_e than that at higher laser energy densities. R_e was enhanced by more than 90% due to higher elastic recovery of the laser-clad layer.

LC using powder feeding of Colmonoy-5 (a nickel base alloy) and Metco-41C (an iron base alloy) on AISI 316L stainless steel and the resulting CE behaviors were investigated in search of Co-free clad layers for applications in nuclear industry [72]. The clad layers were mainly composed of very fine columnar dendritic structures. Compared to 316L, the R_e was improved by a factor of 1.6, 3.7, and 4.1 for laser clad surfaces of Colmonoy-5, Metco-41C, and Stellite-6, respectively. These results demonstrated that Metco-41C is a better choice as a Co-free clad material for potential nuclear applications.

LSA/LC of AISI 316L with NiTi in the forms of powder and strip were reported by Chiu et al [73-75]. NiTi strips are more attractive than powder because the latter is more expensive due to high production cost. For the laser-alloyed 316L with NiTi powder, an alloyed layer was fusion bonded to the substrate without the formation of a brittle interface. The alloyed layer contained Fe as the major constituent element and exhibited an austenitic structure, similar to that of 316L. The R_e of the alloyed layer in deionized water could reach about 29 times that of 316L because of higher surface hardness and elasticity as revealed by nanoindentation tests. However, the superelastic behavior typical of austenitic NiTi was only partially retained and the superior R_e of NiTi was thus still not fully attained due to high degree of dilution. Furthermore, the effect of hydrogen charging on the R_e of the laser-alloyed NiTi layer on 316L, in comparison with 316L and NiTi plate was also studied [74]. Hydrogenation resulted in different degrees of decrease in R_e in all the three types of samples and was ascribed to different causes. For 316L, the hydrogen effect was mild, consistent with the small change in indentation properties. For NiTi-alloyed 316L, the decrease in R_e was due to drop in hardness and elasticity, while for bulk NiTi, the decrease was mainly attributable to the formation of hydrides leading to surface cracks. Moreover, 316L was doubly laser-clad with NiTi strip with *DR* of less than 10% [75]. The clad layer was composed of a NiTi B2 based matrix together with fine precipitates of a tetragonal structure (Fig. 7a). The microhardness of the clad layer was increased from 200 HV of the substrate to about 750 HV due to the dissolution of elements like Fe, Cr and Ni in the matrix.

Nanoindentation tests recorded a recovery ratio near to that of bulk NiTi due to low *DR*. The R_e in deionized water of the doubly clad samples was higher than that of the laser-alloyed sample using NiTi powder and approached that of NiTi plate. The high R_e was attributed to a high hardness, high indentation recovery ratio and the absence of cracks or pores. For untreated AISI 316L, typical ductile fracture was clearly observed on eroded surface and it is consistent with the low hardness and low recovery ratio. Isolated patches of erosion could be observed on the laser-clad 316L with NiTi strip for 12 h, possibly originating from the precipitates (Fig. 7b) [74].

2.2.1.4 LSA of aluminum alloys

LSA of aluminum alloy Al-12Si using pre-mixed powder of Si, Ni, Fe, Cu, Mn, Cr, Co, Mo, and Ti was investigated by Tomlinson and Bransden [76]. The R_e was increased by a factor of 33 times, and the improvement was attributed to a microstructure consisting of densely packed intermetallic compounds. On the other hand, LSA of aluminum alloy AA 6061 using a hardfacing powder NiCrSiB was reported by Man et al. [77], with an increase in R_e of 2 times. The fine dendritic structure of intermetallic compound Ni-Al was responsible for the high hardness (900 HV) of the alloyed layer. It should be pointed out that this hardness is incommensurate with the relatively small increase in R_e.

2.2.1.5 LSA/LC of copper alloys

LC of a Ni-Al bronze with a material of composition similar to that of the base alloy was reported by Hyatt et al. [78]. Owing to the presence of crack-stopping plate-type boundaries in the clad layer, the R_e was increased by 5 times. LSA of brass for improving R_e was investigated by Tam et al [79,80]. Two types of hardfacing powders, Ni-Cr-Al-Mo-Fe and Ni-Cr-Si-B, were flame sprayed on the substrate, followed by laser irradiation. An improvement in R_e of 4.6 folds in the former and 9 folds in the latter was reported. The R_e correlated well with the hardness of the alloyed layers, which in turn depended on the amount of hard phases (e.g. borides) present.

LSA of MAB using Al powder was reported by Tang et al [81]. The alloyed layer was composed of a single η phase (bcc) with hardness higher than 300 HK (Fig. 5c(i)). R_e in deionized water is increased by 30-fold as compared with as-received MAB and 3 times that by LSM. The relatively low R_e of as-received MAB was attributable to its heterogeneous and multi-phased microstructure. Apart from microstructural homogenization, the enhancement in R_e was also related to the increase in microhardness (hard η phase) and the larger grains resulted in less grain boundaries,

which were vulnerable sites for initiation of CE (Fig. 5c(ii)). On the other hand, Kwok et al reported that the R_e of LSA of MAB with Cr, Ni and W was improved by more than two times as compared with that of the MAB substrate due to increase in hardness [82].

2.2.1.6 LSA of NiTi alloy

The R_e of NiTi alloy subjected to laser gas nitriding (LGN) was reported by Cui and his co-workers [83]. The nitrided samples were very resistant to CE. This could be attributed to the high microhardness of the laser-nitrided NiTi alloy, in addition to homogeneous layer with fine grains. In comparison, the R_e of as-received NiTi was lowered by the presence of secondary phases and inclusions, which were initiation sites of cavitation erosion.

2.2.1.7 LSA of titanium alloy

Laser nitriding of Ti6Al4V was reported to be able to significantly increase the R_e in deionised water [57,84]. With increasing nitrogen content of the gas atmosphere in nitriding, the structure within the laser-nitrided layers characteristically changed from martensitic α'-Ti to a fine mixture of α- and β-Ti grains, leading to the formation of different titanium nitrides. The increase of hardness and R_e were mainly attributed to solid solution hardening by nitrogen atoms. It was shown that optimum R_e was achieved in crack-free layers without brittle titanium nitrides [84].

'Among the various couples of added materials and substrate for LSA/LC, LC of austenitic stainless steel 316L with NiTi shows the most significant improvement in R_e in deionized water (43-fold) due to high hardness and high indentation recovery ratio. However, synergistic effect of cavitation erosion and corrosion has not been reported.'

2.2.2 Laser plasma hybrid spraying of titanium alloys with NiTi

In an attempt to fabricate NiTi layer by vacuum plasma spraying of Ni and Ti powders, it was found that due to insufficient mixing, pure metallic powders still remained in the sprayed coating [85]. Consequently, the R_e of the sprayed coatings was less than that of the bulk NiTi. On the other hand, laser plasma hybrid spraying (LPHS) was reported to be capable of synthesizing an intermetallic compound layer from a mixture of pure metallic powders [86,87]. By using LPHS, Hiraga et al. [87,88] successfully deposited a NiTi layer on Ti6Al4V starting from elemental powders of Ni

and Ti. The R_e was increased by a few hundred times. The large increase in R_e was due to a combination of two factors, namely, superelasticity of the austenitic NiTi and high work hardenability.

2.2.3 Laser dispersion – for forming surface composites

Laser dispersion of hard ceramic phase (reinforcement) is a surface modification process that injects hard second phase into a melted substrate. To prevent hard particles from melting, it is necessary to decrease the power or decrease the time the particles spend under the beam. In addition to using lower laser power or higher processing speed, adjusting the hard particle injection nozzle slightly off the beam is an effective way to produce layers with desired thickness and at a reasonable processing speed. These particles remain solid during the process. After solidification, a layer of hard particles dispersed in a matrix on the substrate will become a surface metal matrix composite (MMC) [89] and is in many ways similar to LSA. In order to melt the substrate surface while keeping the hard phase as unmelted powder, the temperature of the melt must be controlled below the melting temperature of the hard phase. For example, the scanning speed may be increased to avoid phase dissolution in the melt. However, rapid solidification of the melt pool with dispersed phase can generate residual stresses leading to cracking of the coating. Nevertheless, cracking may be avoided by preheating the substrate. To achieve a good surface modified layer, the particles must be wetted by the molten substrate material and should also be strongly bound to it. The particles should not dissolve in the molten pool during processing.

Ocelik and his co-workers reported that laser melt injection of ceramics is a feasible technique for the production of protective layer on top of aluminum, titanium and their alloys in the form of MMC coatings [90]. If the melt pool can be extended behind the laser beam, the MMC layers can be created with a gradual change of volume fraction of ceramic particles as ‘functionally graded materials’. However, the formation of the oxide film on the aluminum melt is a barrier for the successful injection into aluminum and its alloys. While injection of WC particles into Ti6A14V substrate causes the formation of new phases (TiC and W_2C) at the particle-matrix interface in the form of a reaction layer. The presence of crystallographic orientation relationships between the WC particle and the new phases formed around it plays an important role in the crack initiation and propagation processes. The excellent bonding between WC particles and Ti6Al4V matrix was confirmed using in-situ tensile test. The sliding wear test at boundary lubrication conditions confirmed good bonding in WC/Ti6Al4V and SiC/AlSi coatings. Compared with the untreated alloys, the wear resistance of SiC/AlSi and of WC/Ti6Al4V coatings is significantly enhanced by 28-32 and 500-1500 times,

respectively. The incorporation of ceramic particles in a metal matrix is a common practice in producing materials for resisting sliding and abrasive wear. However, the efficacy of such a composite system consisting of a matrix with externally added hard reinforcements in resisting CE is controversial. In the investigation on the effect of the hard phase on the CE of ceramic-reinforced aluminum MMC, Tomlinson and Matthews [91] reported that the incubation period was increased in all cases while the erosion rate reduced or unaffected. In an early work by Bhagat [92], it was pointed that the fibres in a ductile matrix/brittle fibre system did not contribute toward increasing R_e. On the other hand, Wei et al. [93] reported that the R_e of the WC reinforced MMC increased with the WC content. The effect of the hard phase on the overall R_e of the MMC depends on quite a number of factors, such as the type, size, and volume fraction of the hard phase, and the conditions of the interface between the matrix and the hard phase.

2.2.3.1 LD of stainless steels with WC

For the laser-fabricated MMC layers on 316L austenitic stainless steel with high volume fractions of ceramic reinforcement [94], R_e was increased by various amounts, ranging from 1.7 to 9.4 times depending on the type of ceramics and the laser parameters used. Microhardness did not correlate well with the R_e in the case of high-volume-fraction MMCs. Rather, interfacial bonding seemed to play a more essential role. By employing composite powders Co-WC and Ni-WC in the laser-fabricated MMC layer on 316L with WC content up to 28 vol.% WC, it was reported that the increase in R_e was much more pronounced, reaching a factor of 45 times in the most favorable case [95]. The presence of Co and Ni not only facilitated the fabrication process, but also improved the properties (stacking-fault energy, strain-induced martensitic transformability, and hardness) of the matrix, in addition to the role played by the ceramic particles.

Likewise, laser surface modification of 316 austenitic stainless steel using coarse WC powder (particle size of 60 μm) and fine WC powder (particle size of 1 μm) for enhancing R_e was further investigated by Lo et al [96,97]. With the coarse WC powder, laser-fabricated MMC layers consisted of 3 to 28 vol.% of WC particles in a γ-FeCrNiW matrix with fine precipitated carbides as shown in Fig. 8a(i) [94]. R_e in 3.5% NaCl solution was found to attain a maximum value (10.7 times that of as-received 316) at 9 vol.% of WC. In such a composite layer, the matrix phase was eroded by ductile fracture and was related to the microhardness, while the WC particles were eroded by brittle fracture initiated at heat-induced defects Fig. 8a(ii).

On the other hand, R_e in 3.5% NaCl solution of the laser-fabricated MMC layers with fine WC powder could reach more than 30 times that of the as-received 316L due

to a microstructure composed of fine carbide dendrites and interdendritic carbide / γ-FeCrNiW eutectic [97] as shown in Fig. 8b(i). The microhardness of the alloyed layer increased with the total W content in the layer. W played an essential role in strengthening the alloyed layer via the formation of precipitated complex carbides and solution hardening. The maximum R_e occurs at a moderate microhardness of approximately 1000 HV and then decreased because the deleterious effect of brittleness becomes prominent at higher hardness. The improvement in R_e was attributed to the increase of W in solid solution and to the precipitation of dendritic carbides, both resulting from the dissociation of the fine WC powder during laser treatment. In contrast to the case of abrasive wear, a microstructure composed of fine precipitated carbides is more resistant to one containing coarse undissolved carbides. Such a microstructure can be achieved by employing fine WC powder as a convenient source of W and C, without involving strategic or polluting elements like Co or Ni [97]. With the use fine WC powder, the hard phases were formed in situ in the MMC. Compared with the as-received AISI 316, cavitation damage of the laser surface-alloyed 316 with fine WC particles was much milder, with the interdendritic region preferentially eroded away, leaving behind a delineated dendritic microstructure as shown in Fig. 8b(ii) [96].

Similarly, laser fabrication of MMC on CrNiMo stainless steel using WC powder was reported by Zhang [98]. The laser formed layer had a dense microstructure, was metallurgically bonded to the substrate, and no crack was present. The CE rate in distilled water of the MMC layer was 0.4 times that of the CrNiMo stainless steel due to the strengthening effect of the precipitate phases W_2C, Ni_4W, $MoNi_4$ and Fe_6W_6C in the γ-FeCrNi matrix. The average hardness of the alloyed layer was 487 HV, which was 1.3 times that of the substrate (380 HV).

The CE behaviour of AISI 420 martensitic stainless steel laser-clad with NiAl–Ni_3Al intermetallic composites (IC) and intermetallic matrix composites (IMC) with TiC reinforcement was investigated by Duraiselvam et al [99]. The R_e of IC and IMC coatings were 3.3 and 3.6 times that of the as-received 420 and 2.4 and 2.6 times that of the heat-treated 420, respectively. The increase in R_e was attributed to the high work hardening ability of the nickel aluminide IC coatings. The resistance was further improved by strengthening the matrix with TiC reinforcement. No correlation was found between R_e and hardness, over the range of process parameters investigated, indicating that the hardness alone cannot improve the R_e. Both the IC and IMC coatings failed due to brittle fracture with varying severity.

2.2.3.2 LD of aluminum alloys with ceramics

The laser-alloyed MMCs of AA6061-SiC and AA6061-Si_3N_4 consisted of small

amounts of Al_4C_3/Al_4SiC_4 and AlN, respectively. For the specimen alloyed with Si_3N_4 (AA6061-Si_3N_4), the R_e was improved by three times as compared with AA6061 because Si_3N_4 has a high fracture toughness. On the other hand there was no significant improvement in R_e of the specimen alloyed with SiC (AA6061-SiC) [100]. The surface hardness of the specimens alloyed with SiC/Si_3N_4 was increased by seven times as compared with AA6061.

2.2.3.3 LD of brass with Ni-Cr-Fe-WC

Laser surfacing of brass with a composite powder Ni-Cr-Fe-WC was reported by Tam et al. [101]. It was concluded that with proper processing parameters, an increase of 9.1 times in R_e could be achieved. A Ni-rich matrix strengthened by precipitated carbides and tightly bound unmelted WC particles was responsible for the high R_e.

2.2.3.4 LD of Ti6Al4V with Ni/Al-TiC and Ni/Al-VC

Duraiselvam and his co-workers reported that TiC reinforced austenitic NiTi (B2)/α_2-Ti_3Al multiphase intermetallic matrix composites (IMC) were laser fabricated on Ti6Al4V using Ni/Al-TiC and Ni/Al-VC powder mixtures [102]. Due to the high content of brittle Ti_2Ni precipitates, the layer laser-modified with Ni/Al-TiC exhibited a few surface cracks which were eliminated by replacing TiC with VC in the starting powder mixture. The former also exhibited a low R_e due to a higher material loss over the pre-existing defects. The coatings exhibited a factor of 1.2–1.8 increase in R_e compared to that of Ti6Al4V. The co-existence of intermetallics in carbide reinforced matrix was responsible for the improved R_e. However, no direct relationship was observed between hardness and R_e of the laser-modified specimens. The failure mode of the modified layers was characterized as brittle fracture.

Among the different examples of laser dispersion of ceramics in the substrate surface layer, dispersion of γ-FeCrNiCo-28%WC on 316L shows the most significant improvement in R_e in 3.5 wt.% NaCl solution (45-fold, higher than that of 316L laser-clad with NiTi) due to low stacking-fault energy, high strain-induced martensitic transformability, and high hardness of the γ-matrix and presence of hard WC particles. Again, synergistic effect of cavitation erosion and corrosion has not been reported.

3 Synergism of cavitation erosion and corrosion of laser-modified surface

In engineering applications, some environments are essentially cavitating, some are essentially corrosive, and some are both cavitating and corrosive. Depending on the process and the material system, the effect of laser surface modification may or may not be beneficial to R_e and corrosion resistance simultaneously. For alloys which are less resistant to CE and corrosion such as carbon steel, laser surface modification benefits the resistance to both CE and corrosion [64]. For alloys which are already corrosion resistant, LSA may improve the R_e but the corrosion resistance may be impaired [103]. For instance, 316L stainless steel possesses superior corrosion resistance due to the chromium oxide on its surface. Some alloying elements or carbides in laser-modified surface could weaken this protective oxide film and thus lower the corrosion resistance. Improvement in R_e at the expense of corrosion resistance is even more common in the case of surface MMC [104]. The difficulty in achieving simultaneous improvement in R_e and corrosion resistance is not unexpected since CE is essentially mechanical in nature while corrosion is electrochemical in nature. Depending on the nature of the environment, a compromise has to be made. In order to elucidate the roles played by mechanical erosion, electrochemical corrosion, and their synergism for mechanism of CE, the pure corrosion rate in a corrosive medium (e.g. in 3.5 wt.% NaCl solution) (C) under quiescent condition, pure CE rate in a non-corrosive medium (e.g. deionized water) (E) and CE rate in the corrosive medium (T) were studied separately according to ASTM G119 and reported in Ref. [105]. The synergism of CE & corrosion (i.e. erosion induced corrosion and corrosion induced erosion) can be calculated by:

$$S = T - E - C$$

The studies of the contribution of S to overall T for the laser-modified samples are discussed as follows:

3.1 LSA of AISI 1050 & 316L with NiCoSiB

By LSA of AISI 1050 & 316L with NiCoCrB (Ni-17.1wt.% Co-19.6wt.% Cr-14.5% Fe-3.5% B-1% C-0.9% Si), the R_e of the laser-alloyed 1050 & 316L in both deionized water and 3.5 wt.% NaCl solution were improved [68,69]. After LSA, the corrosion resistance of 1050 was somewhat increased, owing to the presence of Cr in the alloyed layer, while that of 316L decreased, due to the presence of borides and boro-carbides which weakened the passive film. Corrosion and erosion-corrosion synergism played a significant role in the overall cavitation erosion-corrosion resistance (in NaCl solution). The contributions of corrosion & synergism amounted to approximately (C/T=9.6% and S/T=43.1% respectively) for the laser-alloyed 1050. The corresponding values for laser-alloyed 316L were much lower, but still amounted to approximately

(C/T=2.3 & S/T=18.8%). Thus, it is difficult to simultaneously achieve significant improvements in both R_e and corrosion resistance.

3.2 LSM and LSA of Mn-Ni-Al bronze (MAB)

As mentioned in Sections 2.1.2.5 and 2.2.1.5, the R_e of MAB after LSM and LSA with Al in both deionized water and 3.5 wt.% NaCl solution were enhanced [54,55,81,106]. LSA of MAB with Al brought about an increase in both R_e and corrosion resistance in 3.5% NaCl solution, with a higher increase in comparison with LSM of MAB. The contributions of E, C and S to T of the various MAB samples were shown in Table 4 [106]. For as-received MAB, synergistic effect (S/T=7.2%) was relatively small possibly due to low hardness and the unfavorable microstructure which had made mechanical erosion dominant. Cavitation resulted in enhanced cathodic reaction rate, thus leading to increased corrosion rate (C). For the laser-melted MAB, contribution from synergistic effect (S/T=27.1%) was higher than of as-received MAB and comparable to that reported by Neville et al. and Tomlinson & Talks [107,108]. Cavitation removed or weakened the protective surface film and resulted in enhanced anodic activity and corrosion rate (C). For laser-alloyed MAB, the synergistic effect (S/T) was contributed by corrosion-induced erosion [106]. Moreover, the galvanic effect between the laser-alloyed and as-received MAB was small, this being a favorable factor for justifying the use of LSA with Al as a feasible method in the local surface treatment of MAB.

4 Engineering applications of laser surface modification for combating CE

A recent review was reported by Mann [107] highlighting on experimental investigations of surface modification of hydro and thermal power plant components using a 4.6 kW robotic high-power diode laser (HPDL) system. Mann's studies were mainly focused on HPDL surface treatment of materials and coatings for the hydro and thermal power plant components to combat CE, water droplet erosion and particle erosion. Special emphasis was given on the HPDL surface treatment of martensitic and precipitate-hardened stainless steels, Ti6Al4V alloy, plasma ion nitro-carburized (PINC) layers, high pressure high velocity oxy-fuel (HP-HVOF) WC-10Co4Cr coating and twin-wire arc sprayed (TWAS) SHS 7170 coating which are commonly used in the hydro and thermal power plants. It was reported that HPDL surface treatment eliminates most of the defects present in the PINC layers, HP-HVOF, and TWAS coatings, with improved surface properties, making it a promising potential candidate for hydro and thermal power plants. Particularly, HPDL-treated PINC layers or HPDL-treated

thermally sprayed coatings (HP-HVOF WC-10Co4Cr coating and TWAS SHS 7170 coating) are recommended for combating CE. While higher temperature HPDL-treated martensitic stainless steels and titanium alloy should be used with care because the excessive tensile stresses in the components may lead to shortening of fatigue life. Shot peening followed by HPDL treatment is suggested to be a better option. R_e of HPDL-treated bulk materials and coatings have a good correlation with modified ultimate resilience (*MUR*) as defined below:

$$MUR = UR_{substrate} \times (Hardness_{\ top\ surface}/Hardness_{\ substrate})^2$$

Ultimate resilience (*UR*) is defined as the area of the triangle obtained when the yield point is raised to *UTS* of the engineering stress-strain curve (i.e. $UR = UTS^2/2E$) where *UTS* and *E* are Young's modulus and ultimate tensile strength, respectively.'

On the other hand, Brandt and his co-workers reported that in-situ laser repairing (LC) using Stellite 6 onto turbine blades (AISI 420 martensitic stainless steel) in a power station is feasible and practical using a fiber delivered diode laser and a robot [110] Fig. 9 shows the leading edges of the turbine blades after LC. After one year, the turbine was inspected and the laser-repaired blades showed good performance without sign of damage. Laser surface modification of stainless steel turbine for enhancing R_e was also reported by Yao's group [111,112]. Low-carbon precipitation hardened stainless steel (17-4PH) is widely used to produce steam turbine blades in the power plants due to it with its high strength, high fatigue resistance, excellent corrosion resistance and good weldability. However, under the impact of high-speed steam and water droplets, the blades are prone to CE. The 17-4PH blade was surface-alloyed using a high power CO_2 laser with alloying materials (2.86%Cr, 3.29%Ni, 0.98%Fe, 40.24%W, 51.33 Co). After LSA, the surface layer was denser and the grains were refined, while the microhardness of the surface (average 610 $HV_{0.2}$) was about twice that of the substrate material [111]. The friction coefficient of the laser-alloyed 17-4PH layer was much lower than that of the substrate because of the extremely fine grains and hard phases such as Fe_6W_6C and W_2C. However, the R_e was not evaluated. LSA of steam turbine blades made of 2Cr13 low-carbon martensitic stainless steel using a 7-kW CW CO_2 laser for improving the R_e [112]. The microstructure of surface was refined after LSA which was different from the substrate. The average microhardness after LSA reached 701.2 $HV_{0.2}$ as compared to the substrate (200 - 250 $HV_{0.2}$). The R_e of the laser-alloyed steam turbine blades was increased to twice that of the original blades, which proved that LSA was promising for improving the properties and increasing the lifetime of steam turbine blades.

5. Concluding remarks and future perspectives

From the processing point of view, laser surface modification has already yielded promising results for combating CE. With the advent of more powerful laser systems and appearance of new materials, further development of its applications in the industry is expected in near future. In addition to LTH, LSM, LSA, LC and LD, the field of hybrid laser processing (LPHS) has attracted growing attention recently as it would expand the scope of applicability of laser surface modification [87,88].

From the point of view on selection of a layer/coating fabricated by laser, the response of the protective layer/coating to cavitation attack cannot in general be predicted from conventional mechanical properties owing to the characteristics pertinent to CE. Nevertheless, a few recommendations with respect to R_e can be made from the review above.

(1) High hardness and high toughness are usually beneficial but a hard and brittle surface is detrimental.
(2) A refined and homogeneous microstructure is advantageous.
(3) Structure with high phase transformability or low stacking fault energy is a favorable factor.
(4) Corrosion resistance has to be carefully considered in view of the possible synergistic effect.
(5) For MMCs/IMCs, the strength of the matrix and of interfacial bond is more important than that of the ceramic phase.

Acknowledgements

The work described in this manuscript was fully supported by research grants from the Science and Technology Development Fund (FDCT) of Macau SAR (Grant no. FDCT 070/2011/A3).

References

[1] A. Karimi and J.L. Martin, International Metals Reviews 31 (1986) 1–26.
[2] K.R. Trethewey, T.J. Haley and C.C. Clark, British Journal of Corrosion 23 (1988) 55–60.
[3] R. Garcia, F.G. Hammitt, Journal of Basic Engineering Dec. (1967) 753–763.
[4] R.H. Richman, W.P. McNaughton, Wear, 140 (1990) 63–82.
[5] ASTM G119-09 Standard Guide for Determining Synergism between Wear and Corrosion, ASTM.

[6] C.T. Kwok, F.T. Cheng, H.C. Man, Materials Science and Engineering A290 (2000) 145-154.
[7] H. Jin, F. Zheng, S. Li, C. Hang, Wear 112 (1986) 199–205.
[8] H.J. Amarendra, G.P. Chaudhari, S.K.Nath, Wear 290–291 (2012) 25–31.
[9] T. Lampke, D. Dietrich, A. Leopold, G. Alisch, B. Wielage, Surface and Coatings Technology 202 (2008) 3967-3974.
[10] M.G. Timerbulatov, V. E. Khromov (translated from Vestnik Mashinostroeniya), Wear 38 (1958) 56–58.
[11] C.J. Lin, J.L. He, Wear 259 (2005) 154-159.
[12] C.J. Lin, K.C. Chen, J.L. He, Wear 261 (2006) 1390-1396.
[13] W.F. Wang, M.C. Wang, F.J. Sun, Y.G. Zheng, J.M Jiao, Surface and Coatings Technology 202 (2008) 5116-5121.
[14] F. Cheng, S. Jiang, J. Liang, Applied Surface Science 280 (2013) 287-296.
[15] A. Krella, A. Czyżniewski, Wear 260 (2006) 1324-1332.
[16] C.M. Garzón, H. Thomas, J.F. dos Santos, A.P. Tschiptschin, Wear 259 (2005) 145-153.
[17] J.F. dos Santos, C.M. Garzón, A.P. Tschiptschin, Materials Science and Engineering A382 (2004) 378-386.
[18] H. Li, Z. Cui, Z. Li, S. Zhu, X. Yang, Applied Surface Science 298 (2014) 164-170.
[19] A.N. Allenstein, C.M. Lepienski, A.J.A. Buschinelli, S.F. Brunatto, Wear 309 (2014) 159-165.
[20] A.N. Allenstein, C.M. Lepienski, A.J.A. Buschinelli, S.F. Brunatto, Applied Surface Science 277 (2013) 15-24.
[21] L.A. Espitia, L. Varela, C.E. Pinedo, A.P. Tschiptschin, Wear 301 (2013) 449-456.
[22] C. Godoy, R.D. Mancosu, M.M. Lima, D. Brandão, J. Housden, J.C. Avelar-Batista, Surface and Coatings Technology, 200 (2006) 5370-5378.
[23] S. Hanke, M. Beyer, Aulis Silvonen, J.F. dos Santos, A. Fischer, Wear 301 (2013) 415-423.
[24] F.T. Cheng, K.H. Lo, H.C. Man, Surface and Coatings Technology 172 (2003) 308-315.
[25] Y.Wu, P. Lin, C. Chu, Z. Wang, M. Cao, J. Hu, Materials Letters 61 (2007) 1867-1872.
[26] J. Stella, E. Schüller, C. Heßing, O.A. Hamed, M. Pohl, D. Stöver, Wear 260 (2006) 1020-1027.
[27] W.H. Huang, K.C. Chen, J.L. He, Wear 252 (2002) 459-466.
[28] K.S. Zhou, H. Herman, Surface Technology 18 (1983) 51-62.

[29] C.M. Preece, E.N. Kaufmann, Corrosion Science 22 (1982) 267-281.
[30] W.W. Hu, C.R. Clayton, H. Herman, J.K. Hirvonen, Materials Science and Engineering 45 (1980) 263-268.
[31] K.H. Zum Gahr, Microstructure and Wear of Materials, Elsevier Science Publishers, 1987 (Chapter 8).
[32] W.M. Steen, J. Mazumder, Laser Material Processing, 4th Edn, Springer, London, 2010, .pp. 296-297.
[33] Z. Li, Q. Zheng, J. Li, Journal of Applied Physics 58 (1985) 3860-3864.
[34] Z. Li, J. Zou, Z. Xu, Wear 119 (1987) 13-27.
[35] W.J. Tomlinson, M.G. Talks, Wear (1990) 269-284.
[36] K.H. Lo, F.T. Cheng, H.C. Man, Surface and Coatings Technology 173 (2003) 96–104.
[37] B.S. Mann, JMEPEG 23 (2014) 1964–1972.
[38] C.M. Preece, 'Cavitation Erosion', in: Treatise on Materials Science and Technology, Vol. 16, Erosion, ed. C.M. Preece, Academic Press, (1979) pp. 249-308.
[39] C.T. Kwok, H. C. Man and F. T. Cheng, Materials Science and Engineering A, 242 (1998) 108-120.
[40] W.J. Tomlinson, J.H.P.C. Megaw, A.S. Bransden, M. Girardi, Wear 116 (1987) 249-260.
[41] W.J. Tomlinson, M.G. Talks, Wear 129 (1989) 215-222.
[42] W.J. Tomlinson, M.G. Talks, Wear 139 (1990) 269-284.
[43] W.J. Tomlinson, M.G. Talks, Journal of Materials Science 26 (1991) 804-808.
[44] S.P. Gadag, M.N. Srinivasan, Journal of Materials Processing Technology 51 (1995) 150-163.
[45]. C.M. Preece, C.W. Draper, Wear 67 (1981) 321-328.
[46] B.G. Giren, Surface Engineering 14 (1998) 325-330.
[47] D. Dube, M. Fiset, R. Laliberte, R. Simoneau, Materials Letters 28 (1996) 93-99.
[48] C.M. Preece, C.W. Draper, Wear 67 (1981) 321-328.
[49] C.T. Kwok, H.C. Man and F.T. Cheng, Surface & Coatings Technology 99 (1998) 295-304.
[50] C.T. Kwok, H.C. Man and F.T. Cheng, Surface & Coatings Technology 126 (2000) 238-255.
[51] K.H. Lo, F.T. Cheng, C.T. Kwok, H.C. Man, Materials Letters 58 (2003) 88–93.
[52] M. Matsumura, Y. Isomoto, A. Yabuki, S. Sanui, Corrosion Engineering 40 (1991) 821-826.
[53] C.W. Draper, J.M. Vandenberg, C.M. Preece, C.R. Clayton, Characterization

and Properties of Laser Quenched Aluminum Bronzes, In Proceedings of Conference on Rapidly Solidified Amorphous and Crystalline Alloys, Boston, Nov. 1981, 529-533.

[54] C.H. Tang, F.T. Cheng, H.C. Man, Materials Science and Engineering A373 (2004) 195–203.

[55] C.H. Tang, F.T. Cheng, H.C. Man, Surface and Coatings Technology 182 (2004) 300-307.

[56] R. Cottam, V. Luzin, H. Moody, D. Edwards, A. Majumdar, Y.C. Wong, J. Wang, M. Brandt, Wear 317 (2014) 56–63.

[57] J.M. Robinson, S. Anderson, R.D. Knutsen, R.C. Reed, Materials Science Technology 11 (1995) 611-618.

[58] S. Sarkar, P.M. Raj, S. Chakraborty, G. Phanikumar, K. Chattopadhyay, P. Dutta, Journal of Materials Science 38 (2003) 155-164.

[59] Ehsan Toyserkani, Amir Khajepour, Stephen Corbin, Laser cladding, CRC Press 2005, p.30.

[60] W.J. Tomlinson, S. Bransden, Surface Engineering, 4 (1988) 303-308.

[61] W.J. Tomlinson, S. Bransden, Laser Surface Alloying Grey Iron with Cr, Ni, Co, and Co-Cr Coatings', Surface Engineering, 6 (1990) 281-286.

[62] W.J. Tomlinson, R.T. Moule, J.H.P.C. Megaw, A.S. Bransden, Wear, 117 (1987) 103-107.

[63] C.T. Kwok, H.C. Man and F.T. Cheng, Materials Science and Engineering A, 303 (2001) 250-261.

[64] C.T. Kwok, F.T. Cheng and H.C. Man, Surface & Coatings Technology, 45 (2001) 194-205.

[65] B.G. Giren, M. Szkodo, J. Steller, Wear 258 (2005) 614-622.

[66] M. Szkodo, Journal of Materials Processing Technology 162–163 (2005) 410–415.

[67] C.T. Kwok, F.T. Cheng, H.C. Man, Surface & Coatings Technology 200 (2006) 3544– 3552.

[68] C.T. Kwok, F. T. Cheng, H. C. Man, Surface & Coatings Technology 107 (1998) 31-40.

[69] C.T. Kwok, F. T. Cheng, H. C. Man, Materials Science and Engineering A290 (2000) 74-88.

[70] M. Szkodo, Journal of Achievements in Materials and Manufacturing Engineering 18 (2006) 240-242.

[71] R. Singh, D. Kumar, S.K. Mishra, S.K. Tiwari, Surface & Coatings Technology 251 (2014) 87–97.

[72] C.P. Paul, B.K. Gandhi, P. Bhargava, D.K. Dwivedi, L.M. Kukreja, Journal of

Materials Engineering and Performance 23 (2014) 4463-4471.
[73] K.Y. Chiu, F.T. Cheng, H.C. Man, Materials Science and Engineering A392 (2005) 348–358.
[74] K.Y. Chiu, F.T. Cheng, H.C. Man, Materials Letters 61 (2007) 239–243.
[75] K.Y. Chiu, F.T. Cheng, H.C. Man, Materials Science and Engineering A402 (2005) 126–134.
[76] W.J. Tomlinson, S. Bransden, Surface Engineering 11 (1995) 337-344.
[77] H.C. Man, S. Zhang, T.M. Yue, F.T. Cheng, Surface and Coatings Technology, 148 (2001) 136-142.
[78] C.V. Hyatt, K.H. Magee, T. Betancourt, Metallurgical and Materials Transactions A29 (1998) 1677-1690.
[79] K.F. Tam, F.T. Cheng, H.C. Man, Materials Science and Engineering A325 (2002) 365-374.
[80] K.F. Tam, F.T. Cheng, H.C. Man, Surface & Coatings Technology 149 (2002) 36-44.
[81] C.H. Tang, F.T. Cheng, H.C. Man, Surface & Coatings Technology 200 (2006) 2602– 2609.
[82] C.T. Kwok, P.K. Wong, W.K. Chan, F.T. Cheng, H.C. Man, Laser Surface Alloying of Mn-Ni-Al Bronze for Cavitation Erosion Resistance, Proceedings of the 29th International Congress on Applications of Lasers & Electro-Optics 2010 (ICALEO '10), Miami, USA, 2010, (paper no. 1105).
[83] Z.D. Cui, H.C. Man, F.T. Cheng, T.M. Yue, Surface and Coatings Technology 162 (2003) 147–153.
[84] J. Kaspar, J. Bretschneider, S. Jacob, S. Bonß, B. Winderlich and B. Brenner, Surface Engineering, 23 (2007) 99-106.
[85] K.S. Zhou, D.Z. Wang, M. Liu, Thermal Spray Adv. Coat. Technol. (1988) 167-174.
[86] S. Sasaki, Surf. Eng. 13 (1997) 238-242.
[87] H. Hiraga, T. Inoue, H. Shimura and A. Wear, 231 (1999) 272-278.
[88] H. Hiraga, T. Inoue, S. Kamado, Y. Kojim, A. Matsunawa, H. Shimura, Surface and Coatings Technology 139 (2001) 93-100.
[89] J.D. Ayers, R.J. Schaefer, W.P. Robey, J Met 19 (1980) Aug.
[90] V. Ocelik, S. Nijman, R. van Ingen, U. Oliveira, J. Th.M. De Hosson, Laser melt injection of hard ceramic particles into Al and Ti alloys - processing, microstructure and mechanical behavior, Transaction WIT Transactions on Engineering Sciences, Surface Treatment VI, 39 (2003) 14.
[91] W.J. Tomlinson, S.J. Matthews, Journal of Materials Science Letters 13 (1994) 170-173.

[92] R.M. Bhagat, Journal of Materials Science Letters 6 (1987) 1473-1475.
[93] J. Wei, F.X. Wang, Y.Q. Cheng and N.P. Chen, Journal of Tribology 115 (1993) 285-288.
[94] F.T. Cheng, C.T. Kwok and H. C. Man, Surface & Coatings Technology 139 (2001) 14-24.
[95] F.T. Cheng, C.T. Kwok, H.C. Man, Materials Letters 57 (2002) 969-974.
[96] K.H. Lo, F.T. Cheng, H.C. Man, Materials Science & Engineering A357 (2003) 168-180.
[97] K.H. Lo, F.T. Cheng, C.T. Kwok, H.C. Man, Surface & Coatings Technology 165 (2003) 258-267.
[98] X.B. Zhang, C.S. Liu, X.D. Liu, J. Donga, B. Yu, International Journal of Minerals, Metallurgy and Materials 16 (2009) 203–207.
[99] M. Duraiselvam, R. Galun, V. Wesling, .B.L. Mordike, R. Reiter, J. Oligmüller, Surface & Coatings Technology 201 (2006) 1289–1295.
[100] H.C. Man, C.T. Kwok, T.M. Yue, Surface & Coatings Technology 132 (2000) 11-20.
[101] K.F. Tam, F.T. Cheng, H.C. Man, Materials Research Bulletin 37 (2002) 1341-1351.
[102] M. Duraiselvam, R. Galun, V. Wesling, B.L. Mordike, .R. Reiter, J. Oligmöller, G. Buvanashekaran, Materials Science and Engineering A454–455 (2007) 63–68.
[103] C.T. Kwok, F.T. Cheng, H.C. Man, Materials Science & Engineering A290 (2000) 55-73.
[104] K.H. Lo, F.T. Cheng, C.T. Kwok, H.C. Man, Journal of Laser Applications 15 (2003) 107-114.
[105] Standard Guide for Determining Synergism Between Wear and Corrosion, G119-04, Annual Book of ASTM Standards, Vol. 03.02, ASTM, Philadelphia, 2004.
[106] C.H. Tang, F.T. Cheng, H.C. Man, Surface & Coatings Technology 200 (2006) 2594– 2601.
[107] B.S. Mann, JMEPEG 24 (2015) 4488–4502.
[108] A. Neville, T. Hodgkiess, J.T. Dallas, Wear 186/187 (1995) 497–507.
[109] W.J. Tomlinson, M.G. Talks, Ultrasonics 29 (1991) 171–175
[110] M. Brandt, J. Harris, C. Chipperfield, In-situ laser repair of steam turbine blades, Proceedings of the Fourth International WLT-Conference on Lasers in Manufacturing 2007, Munich, June 2007
[111] J. Yao, L. Wang, Q. Zhang, F. Kong, C. Lou, Z. Chen, Optics and Laser technology 40 (2008) 838-843.

[112] J. Yao, L. Wang, C. Yu, F. Kong, Q. Zhang, C. Lou, J. Fu, Cavitation Resistance of Steam Turbine Blades after Laser Alloying, in Challenges of Power Engineering and Environment, International Conference on Power Engineering, Hangzhou, 2007, 1054-1058.

Table 1. Summary of studies on LTH for improving R_e.

Material	Findings	Investigators	Year
High-phosphorous cast iron	R_e increased by 1.9 times, due to formation of a hard martensitic layer.	Li et al. [33]	1985
CrMoCu alloy cast iron	Improvement was very small.	Li et al. [34]	1987
Cr cast iron	Erosion rate was reduced by about 10%, but less effective than in LSM.	Tomlinson & Talks [35]	1990
440C martensitic stainless steel	LTH was more effective than LSM in enhancing R_e and corrosion resistance as compared with conventional heat treatment. Re increased by about 3 times.	Lo et al. [36]	2003
13Cr4Ni PH stainless steel	The R_e have improved significantly after laser treatment due to its increased surface hardness and formation of fine-grained microstructure. R_e was correlated with microstructure and mechanical properties such as ultimate tensile strength, modified ultimate resilience, and microhardness.	Mann [37]	2014

Table 2. Summary of studies on LSM for improving R_e.

Material	Findings	Investigators	Year
Cast irons	(i) For high-phosphorous cast iron, R_e increased by a factor of 2.3. (ii) For CrMoCu alloyed cast iron, improvement was small.	Li et al. [33], Li et al. [34]	1985, 1987
Cast irons	(i) R_e in distilled water increased by 2 to 20 times, depending on type of cast iron. (ii) Improvement attributed to removal of graphite flakes. (iii) Improvement much lower in 3 % salt water, mainly due to corrosion-enhanced erosion.	Tomlinson et al. [40-43]	1987, 1989, 1990, 1991
Ductile iron	R_e increased by at least 6 times in corrosive water media.	Gadag & Srinivasan [44]	1995
Medium carbon Steels	(a) For 1040, enhancement of R_e (about 2.8 times) was due to formation of martensitic layer. (b) For steel 1045, the improvement was similar.	Preece & Draper [45] Giren [46]	1981 1998
IRECA steel	Re increased by 3 times, attributable to a refined microstructure	Dube et al. [47]	1996
Austenitic stainless steel	For 303, *Re* was lowered due to surface roughening and residual stress.	Preece & Draper [48]	1981

Austenitic & duplex stainless steels	For S31603, *Re* increased by 23 %, perhaps due to presence of residual tensile stress. (ii) For 30400 and 32760, R_e was lowered due to compressive residual stress and high δ-ferrite content, respectively.	Kwok et al [49]	1998
420 martensitic stainless steel	R_e was 1.8 times that of heat-treated samples due to high volume fraction of retained austenite.	Kwok et al [50]	2000
440C Martensitic stainless steel	Compared with conventional hardening, the R_e achieved by LSM was improved in deionized water (by a factor of 1.95) but reduced in NaCl (by a factor of 0.48).	Lo et al. [51]	2003
Al bronzes	(i) incubation period increased by an order of magnitude. (ii) steady-state erosion rate reduced by 2.6 times.	Draper et al. [53]	1982
Mn-Ni-Al bronze (MAB)	(i) significant reduction in the pure erosion rate (*E*), corrosion rate (*C*), and cavitation erosion–corrosion rate (*T*) in 3.5 wt.% NaCl solution, with reduction factors amounting to 8.89, 1.92 and 5.30, respectively. (ii) The erosion resistance benefited from a homogeneous & single-phase microstructure resulting from LSM.	Tang et al [54]	2004
Mn-Ni-Al bronze (MAB)	(i) R_e of MAB in 3.5 wt.% NaCl solution is significantly improved, with a maximum value reaching 5.8 times that of untreated MAB or 2.2 times that of untreated NAB. (ii) The enhancement in erosion resistance by laser treatment results from an increase in hardness and homogenous and refined single-phase (β) microstructure. The erosion resistance peaks at an intermediate hardness, evidencing that hardness is not the sole factor in determining the R_e.	Tang et al [55]	2004
Ni-Al bronze (NAB)	(i) The weight loss after 4 h of testing has decreased from 0.027 g to around 0.002 g for both types of laser treatment (LSM and laser-processed), a 1350% increase in the performance. (ii) It is apparent that the two types of laser treatment have similar CE rates of 0.0037 g for the laser-processed NAB and 0.0038 g for the laser-melted NAB after 6-h testing.	Cottam [56]	2014

Ti-6Al-4V	R_e was unaffected by LSM in Argon.	Robinson et al. [57]	1995

Table 3. Summary of studies on LSA/LC for improving R_e.

Substrate	Additional materials	Findings	Investigators	Year
Grey cast iron	Cr	The coating reduced the steady state erosion rate of cast iron in distilled and salt waters to 0.04 and 0.11 of the uncoated level respectively.	Tomlinson & Bransden [60]	1988
Grey cast iron	Cr, Ni, Co, Co-Cr	(i) Ranking of R_e: Cr > Co-Cr > Ni > as-received cast iron. (ii) R_e increased by 25 and 9 times in distilled water and 3% NaCl solution respectively.	Tomlinson & Bransden [61]	1990
1050 carbon steel	Ni- and Co-based hardfacing alloy	R_e improved due to increased hardness and a fine microstructure.	Tomlinson et al. [62], Kwok et al [63]	1987 2001
1045 carbon steel, 2Cr13 chromium steel	Mn, Cr, Ni, Si, Ti, Co, Nb, Al, Mo, B powder	The improvement depends on the work-hardening capability of the alloyed layer.	Giren et al [65]	2005

1045 carbon steel	Mn, Ni, Cr, Nb, Mo, and Co	Higher resistance was achieved if steel microstructures were susceptible to strain hardening due to presence of some amount of austenite.	Szkodo [66]	2005
1050 carbon steel	Al	The R_e of the laser-aluminized 1050 was higher than that of the substrate (about 17 times) due to the presence of Fe_3Al, FeAl, and solid solution hardened α-ferrite.	Kwok et al [67]	2006
316L stainless steel	NiCrSiB	For 316, R_e was enhanced up to 7.7 times due to increase in hardness by the uniformly dispersed and fine secondary phases (borides and boro-carbides)	Kwok et al [68]	1998
316L Stainless steel	NiCoCrB, Cr, Mo, C, Co, Ni, Mn, AlSiFe, Si, Si_3N_4	R_e increased by 12 folds in the best case, attributable to increase in hardness and lowering of SFE, etc.	Kwok et al [63,69]	2001 2000
X5CrNi18-10 stainless steel	Fe-Cr-Mn, Fe-Cr-Co	Structure refinement due to laser processing contributes to delaying of austenite → martensite phase transformation. Kinetic of austenite → martensite transformation is different for investigated alloys and depends on the chemical composition and laser processing conditions.	Szkodo [70]	2006
13Cr-4Ni Stainless steel	Stellite 6	R_e was enhanced by more than 90% after LC due to elastic recovery of the laser-clad layer.	Singh [71]	2014
316L Stainless steel	Colmonoy-5 (nickel base alloy), Metco-41C (iron base alloy), Stellite-6	The cavitation erosion behaviors of laser clad layers were compared to that of Stellite-6. The cavitation erosion resistance was improved by a factor of 1.6, 3.7, and 4.1.	Paul [72]	2014
316L Stainless steel	NiTi powder	The R_e of the alloyed layer in deionized water could reach about 29 times that of 316L because of higher surface hardness and elasticity	Chiu et al [73]	2005

316L Stainless steel	NiTi powder	Hydrogenation resulted in different degrees of decrease in R_e is ascribed to different mechanisms. For 316L, the hydrogen effect was mild, consistent with the small change in indentation properties. For NiTi-alloyed 316L, the decrease in R_e was owing to a drop in hardness and elasticity, while for bulk NiTi, the decrease was mainly attributable to the formation of hydrides leading to the presence of surface cracks.	Chiu et al [74]	2007
316L Stainless steel	NiTi strips	The R_e in deionized water of the doubly clad samples is higher than that of the laser-alloyed sample with NiTi powder and approaches that of NiTi plate. It is attributed to a high hardness, high indentation recovery ratio and the absence of cracks or pores.	Chiu et al [75]	2005
Al-12%Si	Fe, Ni, Mn, Cu, Cr	Enhancement of R_e was due to densely packed intermetallic compounds.	Tomlinson & Bransden [76]	1995
AA6061	NiCrSiB	R_e doubled, due to presence of Ni-Al.	Man et al. [77]	2001
Ni-Al bronze	Ni-Al bronze wire	R_e increased by 5 times, due to presence of crack-stopping plate-type boundaries.	Hyatt et al. [78]	1998
Brass	(i) Ni-Cr-Al-Mo-Fe, (ii) Ni-Cr-B-Si	R_e improved by (i) 4.6 and (ii) 9 times respectively, due to presence of hard phases.	Tam et al [79,80]	2002
Mn-Ni-Al bronze	Al	R_e in deionized water is increased by a 30-fold as compared with as-received MAB and 3 times that by LSM.	Tang et al [81]	2006
Mn-Ni-Al bronze	Cr, Ni, Mo, W	R_e of LSA of MAB with Cr, Ni and W was improved by more than two times as compared with that of the MAB substrate due to increase in hardness	Kwok et al [82]	2010
NiTi	N_2	R_e of the laser-nitrided NiTi is attributed to the high hardness of the TiN surface layer.	Cui et al [83]	2003

Ti-6Al-4V	N_2 (0-20%)	Enhancement of R_e was due to nitrogen-alloyed α structure, but not to the continuous TiN layer.	Robinson et. al. [57]	1995
Ti–6Al–4V	N_2 (0-25%)	Increase in hardness and R_e was mainly attributed to solid solution hardening of the nitrogen. Optimum R_e was only achieved if crack free layers contain no brittle titanium nitrides.	Kaspar et al [84]	2007
Ti-6Al-4V	Ni, Ti powder	R_e increased by a few hundred times, due to superelasticity and high work hardenability.	Hiraga et al [87,88]	1999 2001

Table 4. Summary of studies on LD improving R_e.

Substrate	Additional materials	Findings	Investigators	Year
316L austenitic stainless steel	WC, Cr_3C_2, SiC, TiC, CrB_2, Cr_2O_3	R_e increased by 1.7 to 9.4 times. Interfacial bond strength rather than hardness was important.	Cheng et al [94]	2001
316L austenitic stainless steel	Co-WC, Ni-WC	R_e increased by 45 times, due to improvement of matrix properties and presence of WC particles.	Cheng et al [95]	2002
316 austenitic stainless steel	Coarse WC powder	R_e depends on the volume fraction of WC, and could reach about 10.8 times that of substrate.	Lo et al [96]	2003
316 austenitic stainless steel	Fine WC powder	R_e may reach as high as 30 times due to W in solid solution and fine carbides.	Lo et al [97]	2003

CrNiMo stainless steel	WC	The cavitation erosion mass loss rate of the laser-alloyed layer was only 0.4 times that of the CrNiMo stainless steel due to its metallurgical combination and the strengthening effects of the precipitate phases.	Zhang et al [98]	2009
420 martensitic stainless steel	NiAl, TiC	The R_e of IC and IMC coating was 3.3 and 3.6 times that of the as-received specimen and 2.4 and 2.6 times that of the heat-treated specimen, respectively. The increase in R_e was attributed to the high work hardening ability of the nickel aluminide IC coatings. The resistance was further improved by strengthening the matrix with TiC reinforcement.	Duraiselvam et al [99]	2006
AA6061	SiC and Si_3N_4	R_e increased by 3 times, due to increase in hardness.	Man et al. [100]	2000
Brass	Ni-Cr-Fe-WC	R_e improved by 9.1 times, due to a strong matrix and a strong bonding between matrix and WC	Tam at al [101]	2002
Ti6Al4V	Ni/Al–TiC and Ni/Al–VC	The coatings exhibited a factor of 1.2–1.8 increase in R_e compared to that of Ti6Al4V due to the co-existence intermetallics in carbide reinforced matrix.	Duraiselvam et al [102]	2007

Table 5. Contributions of *E, C* and *S* of various samples of MAB [104].

Sample	*E/T (%)*	*C/T (%)*	*S/T (%)*
MAB (As-received)	92.6	0.2	7.2
MAB (LSM)	72.1	0.8	27.1
MAB (LSA with Al)	28.3	1.0	70.7

Figures

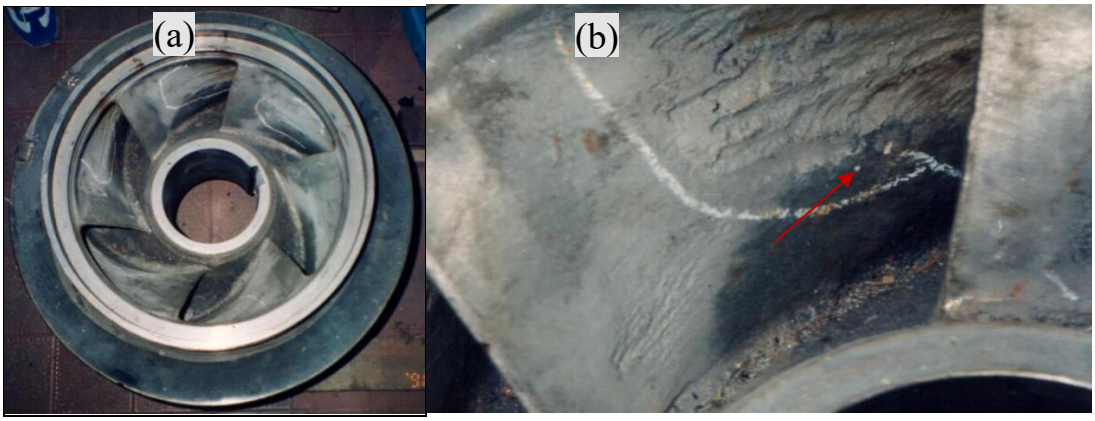

Fig. 1(a) Water pump impeller made of AISI 316 stainless steel (b) cavitation damage in impeller vane.

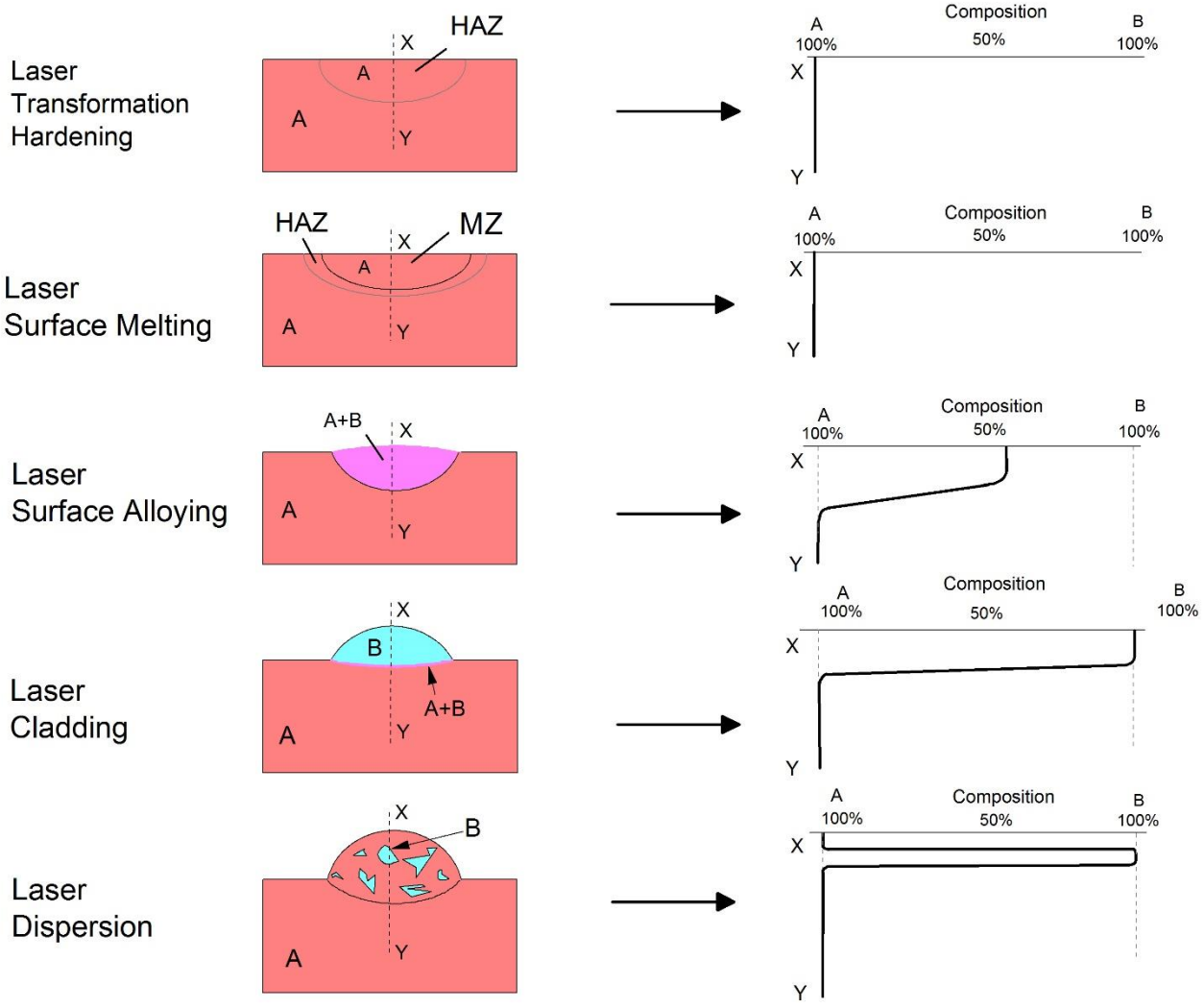
Laser
Transformation
Hardening
HAZ
X
A
A
Y
Composition
A
100%
50%
B
100%
X
Y
Laser
Surface Melting
HAZ
MZ
X
A
A
Y
Laser
Surface Alloying
A+B
X
A
Y
Laser
Cladding
X
B
A+B
A
Y
Laser
Dispersion
X
B
A
Y

Fig. 2. Schematic of various types of laser surface modification for combating cavitation erosion. The diagrams on the left show the compositional profiles from the laser-modified zones down to the substrate along XY.

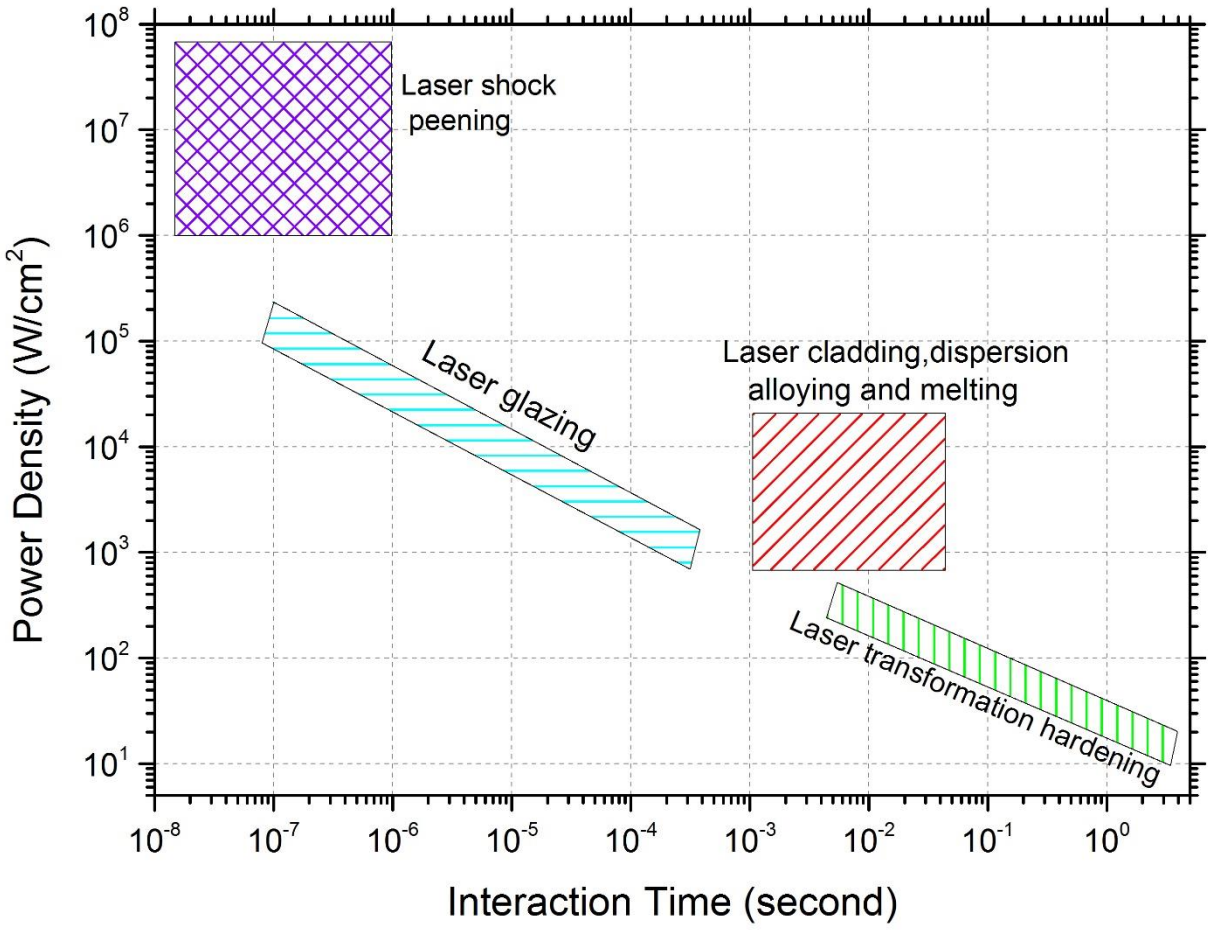

Fig 3. Operational regimes of laser surface modification.

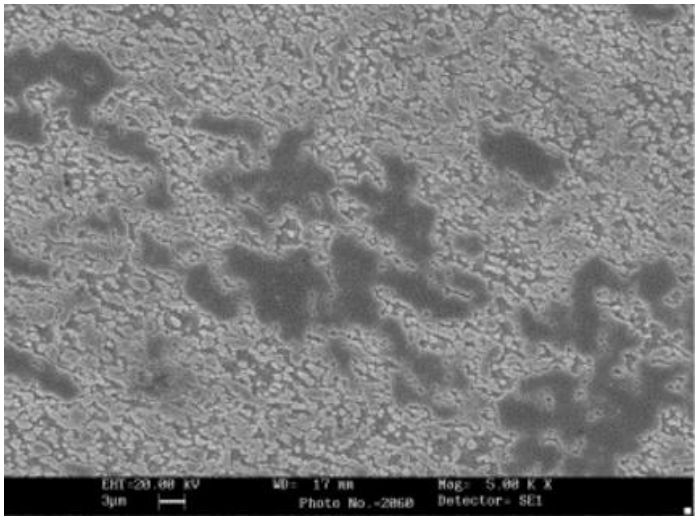
EHT=20.00 kV
WD= 17 mm
Mag= 5.00 K X
3µm
Photo No.=2060
Detector= SE1

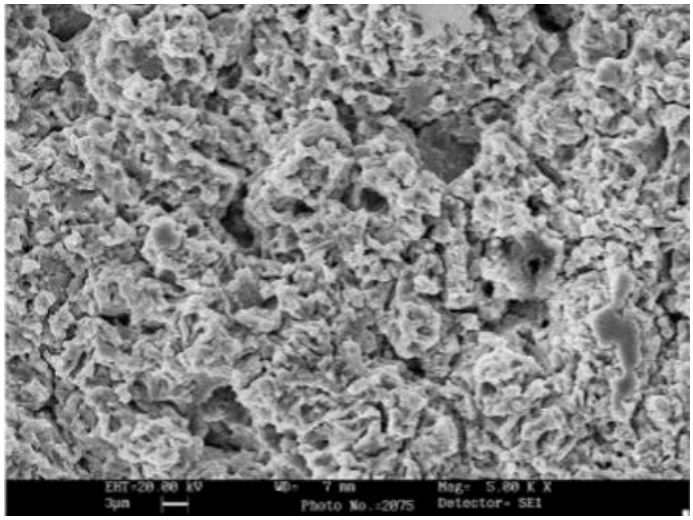
EHT=20.00 kV
WD= 7 mm
Mag= 5.00 K X
3µm
Photo No.=2075
Detector= SE1

(a)(i) (a)(ii)

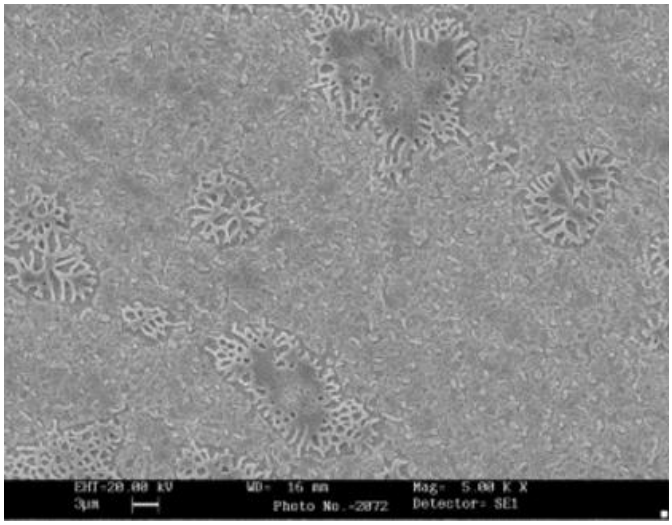
EHT=20.00 kV
WD= 16 mm
Mag= 5.00 K X
3µm
Photo No.=2072
Detector= SE1

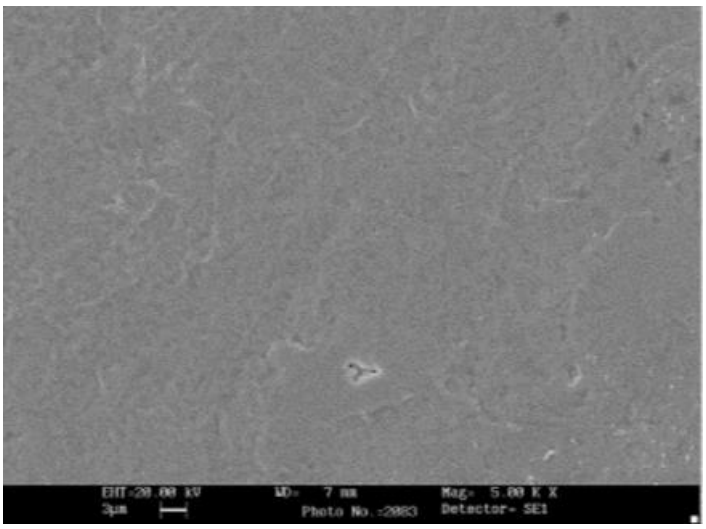

(b)(i) (b)(ii)

Fig. 4. SEM micrographs of (a)(i) as-received martensitic stainless 440C and (a)(ii) after cavitation erosion in 3.5 wt.% NaCl solution for 4 hours; (b)(i) laser-transformation hardened 440C and (b)(ii) after cavitation erosion in 3.5 wt.% NaCl solution for 4 hours [36].

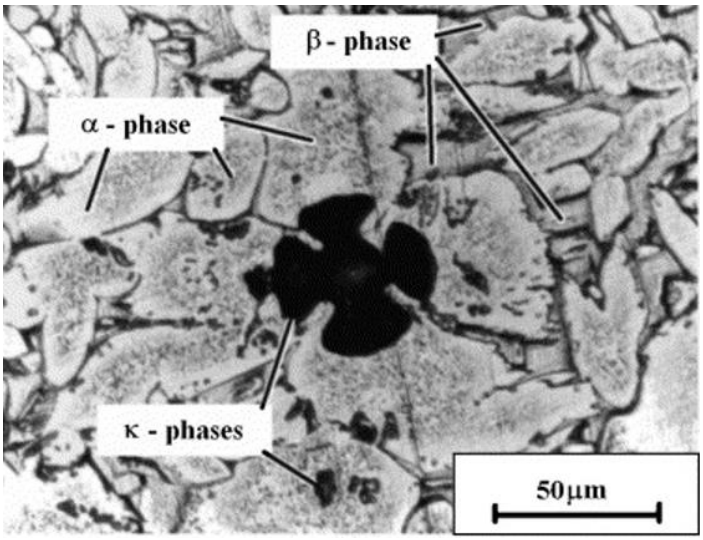
β - phase
α - phase
κ - phases
50μm

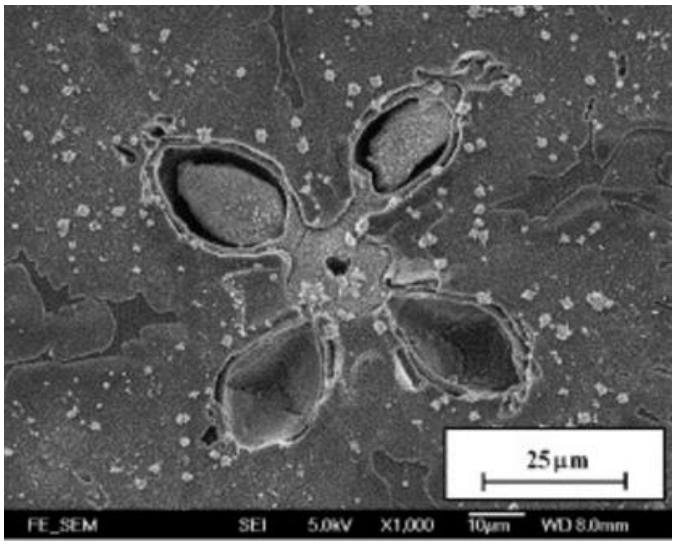
25μm
FE_SEM SEI 5.0kV X1,000 10μm WD 8.0mm

(a)(i) (a)(ii)

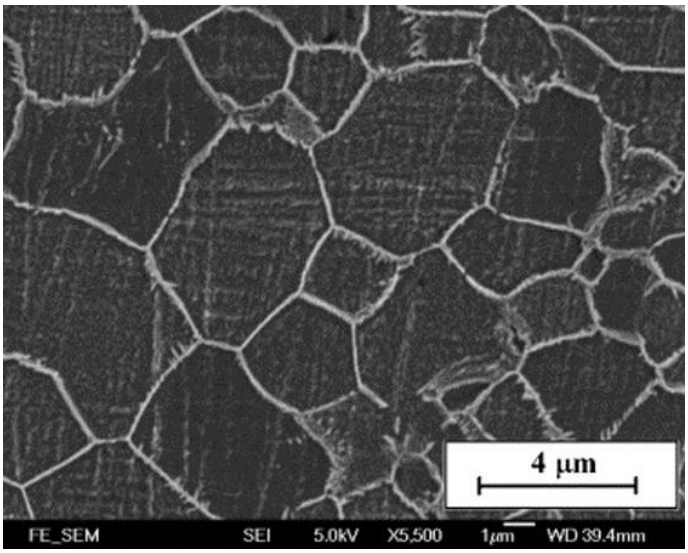
4 μm
FE_SEM SEI 5.0kV X5,500 1μm WD 39.4mm

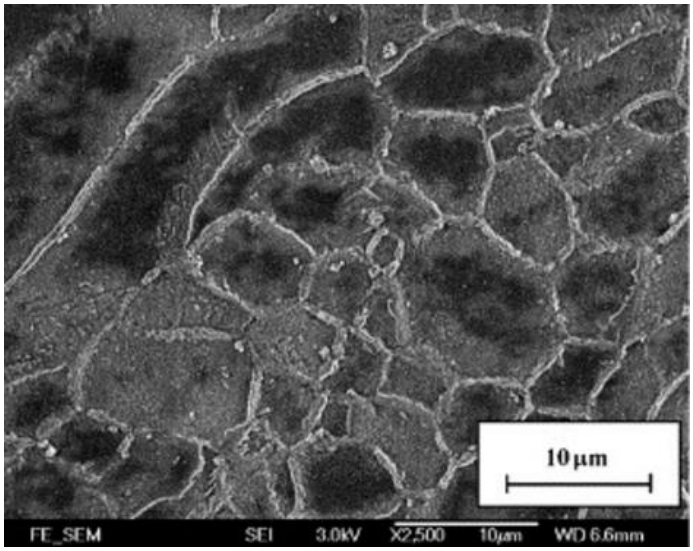
10 µm
FE_SEM SEI 3.0kV X2,500 10µm WD 6.6mm

(b)(i)

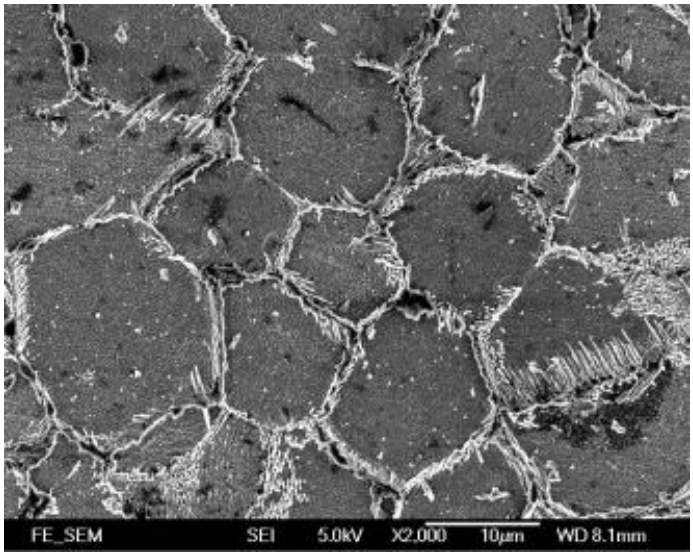
FE_SEM SEI 5.0kV X2,000 10µm WD 8.1mm

(b)(ii)

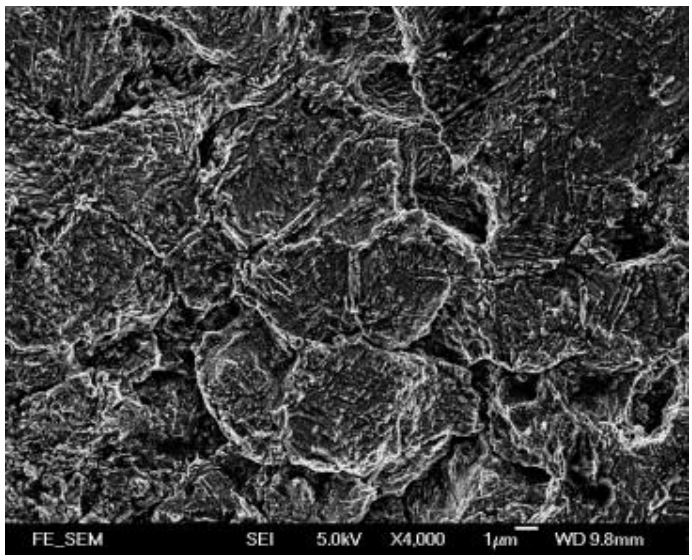
FE_SEM SEI 5.0kV X4,000 1µm WD 9.8mm

(c)(i)

(c)(ii)

Fig. 5. Micrographs of (a)(i) as-received MAB (optical micrograph) and (a)(ii) after cavitation erosion in 3.5 wt.% NaCl solution for 5 days (SEM micrograph) (b)(i) laser surface-melted MAB (SEM micrograph) and (a)(ii) surface after cavitation erosion in 3.5 wt.% NaCl solution for 5 days (SEM micrograph) [54] and laser surface-alloyed MAB with Al (SEM micrograph) and (a)(ii) surface after cavitation erosion in 3.5 wt.% NaCl solution for 12 hours (SEM micrograph) [55].

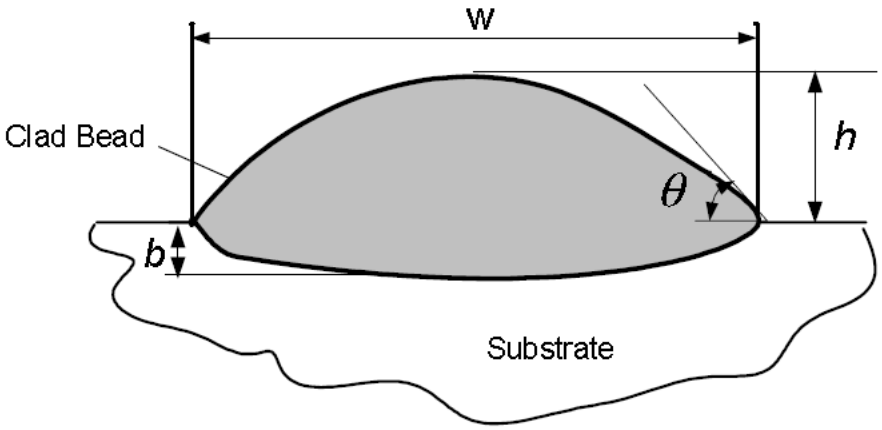

Fig. 6. Schematic diagram of cross-section through an alloyed / clad bead [107].

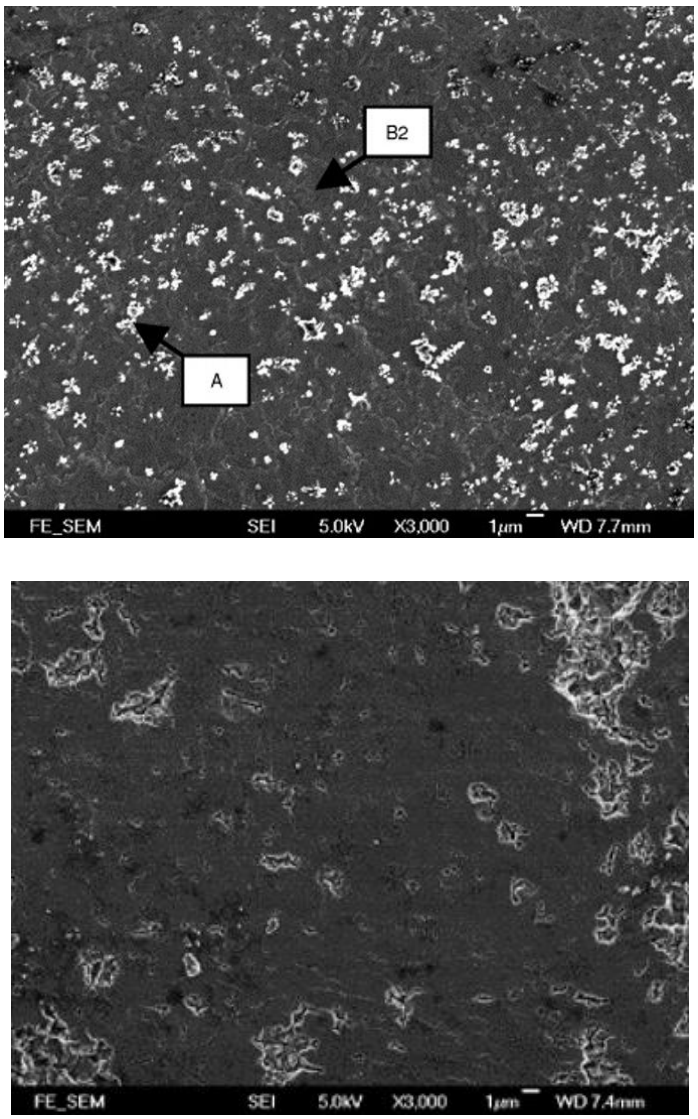

(a) (b)

Fig. 7. SEM micrographs showing microstructure of laser-clad 316L with NiTi strip; the major phase present is the B2 phase with a minor phase minor phase corresponds to the small precipitates (marked A); and (b) after cavitation erosion in 3.5 wt.% NaCl solution for 24 hours [75].

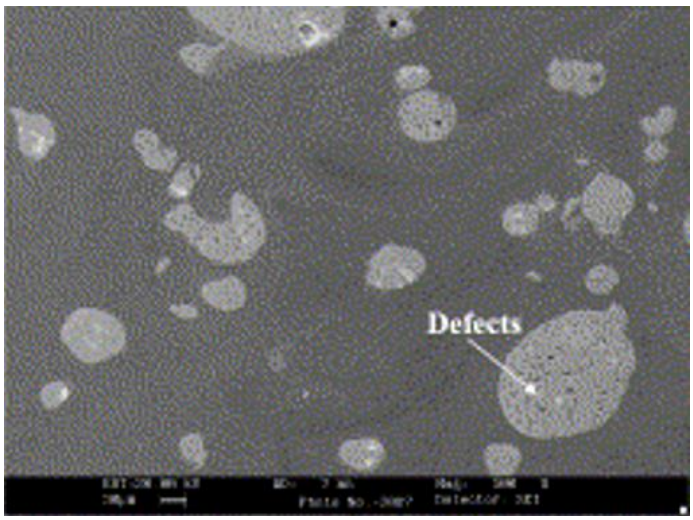

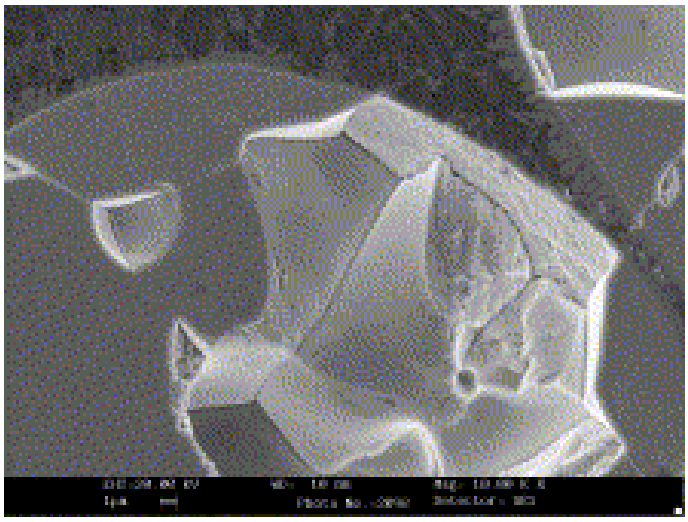

(a)(i) (a)(ii)

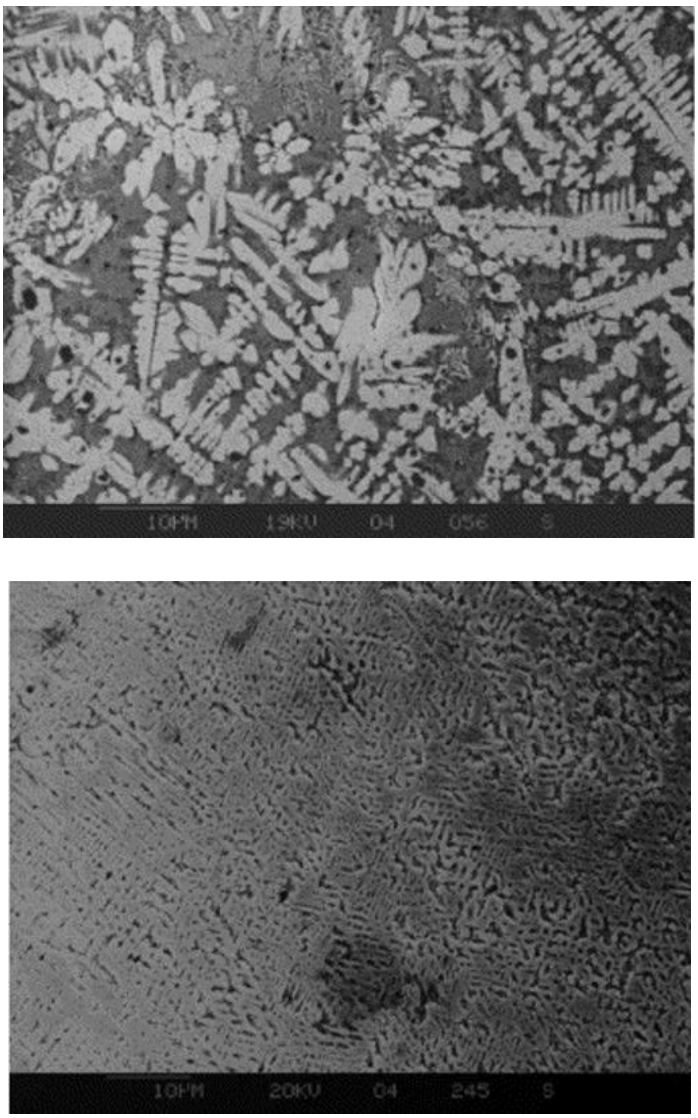

(b)(i) (b)(ii)

Fig. 8. SEM micrographs of (a)(i) laser surface-alloyed 316 with coarse WC particles and (a)(ii) after cavitation erosion in 3.5 wt.% NaCl solution for 15 min (note the brittle fracture on the WC surface) [96]; (b)(i) laser surface-alloyed 316 with fine WC particles and (b)(ii) after cavitation erosion in 3.5 wt.% NaCl solution for 240 min [97].

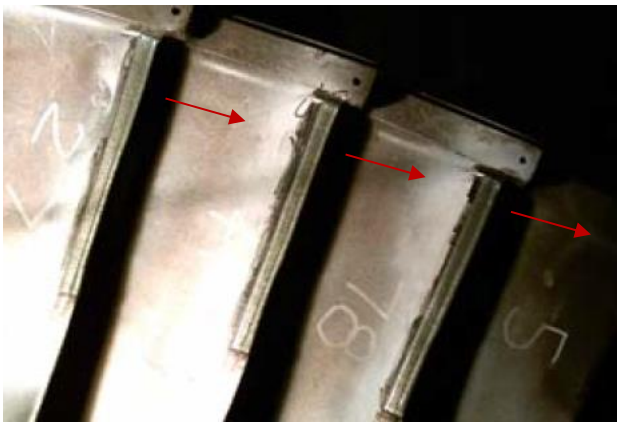

Fig. 9. AISI 420 martensitic stainless steel turbine blades laser-clad with Stellite 6 [110].